AADE-11-NTCE-46



Advances in Swab-Surge Modeling for Managed Pressure Drilling

Wilson Chin and Xiaoying Zhuang, Stratamagnetic Software, LLC

Copyright 2011, AADE

This paper was prepared for presentation at the 2011 AADE National Technical Conference and Exhibition held at the Hilton Houston North Hotel, Houston, Texas, April 12-14, 2011. This conference was sponsored by the American Association of Drilling Engineers. The information presented in this paper does not reflect any position, claim or endorsement made or implied by the American Association of Drilling Engineers, their officers or members. Questions concerning the content of this paper should be directed to the individual(s) listed as author(s) of this work.

Abstract

Conventional swab-surge calculations, crucial to job planning and safe drilling, are deficient in several respects. In modern horizontal wells, typically miles in length, high annular borehole eccentricities are the rule; existing methods unrealistically assume, for simplicity, concentric boreholes, and predict pressure drops largely inconsistent with tripping speeds. Most models also assume that mud circulation ceases, a premise no longer true in managed pressure drilling operations with continuous circulation. These errors are problematic to steady flows, but transient flows take even more damaging assumptions. "Water hammer" approaches (also using the inadequate assumptions noted) apply classical acoustic solutions assuming sudden valve closures or piston excitation. Since drillstrings are long and heavy, transient effects focusing on constant density, inertia-dominated effects are more likely in practice, but few models address this limit. We present new steady and transient models for swab-surge analysis encompassing several important drilling variables: high annular eccentricity, non-Newtonian flow where yield stress is important (with correct predictions for pressure drop and plug zone size and shape), and simultaneous mudpump circulation. The new methods, rigorously formulated and quickly solved on curvilinear meshes to accommodate cuttings bed and washout geometries, provide the accuracy and confidence needed to drill in ultradeep waters.

Introduction

Non-Newtonian flows in highly eccentric annuli with cuttings beds, washouts and fractures, encountered in cementing and managed pressure (and underbalanced) drilling, are solved without crude slot flow and hydraulic radius approximations. The nonlinear partial differential equations, written to customized, boundary-conforming, curvilinear coordinate grid systems providing high physical resolution in tight spaces, are solved exactly with no-slip conditions, and detailed velocity, apparent viscosity, shear rate and viscous stress fields are computed for pressure drop, hole cleaning and other applications. For fluids with yield stress, well known uncertainties related to plug zone size and shape are fully resolved using Herschel-Bulkley relations applicable across transition boundaries (determined iteratively as part of the solution) reaching into and across the plug. Two-dimensional, single-phase, steady flow simulations, solved rapidly using finite difference methods, provide detailed numbers and color displays for all physical quantities within seconds, with excellent numerical stability for all fluid types with and without yield stress. Formulations for steady-state casing or drillpipe longitudinal translation and rotation are presented, and extensions to model transient incompressible effects associated with starting, stopping and periodic movement, important in evaluating cement-mud displacement efficiency, axial-helical cuttings transport, swab-surge, and jarring remedies for freeing stuck pipe, are developed. Practical problems are presented and the advantages over existing models are described.

In this paper, extensive calculation methods and new modeling capabilities are presented for job planning and swabsurge predictive analysis in modern managed pressure drilling applications.

Background

Annular flow modeling in boreholes, important to both drilling and cementing, is as old as petroleum engineering itself. In the simplest case, flow configurations are represented by concentric circles through which steady, two-dimensional, Newtonian and power law fluids flow; in these limits, exact analytical or numerical solutions of the flow equations provide useful tools for operational applications. For more complicated problems, e.g., eccentric annuli, non-ideal geometric irregularities, non-Newtonian yield stress fluids, pipe translation and rotation, however, numerous mathematical obstacles arise, which unfortunately introduce inefficiencies into field practices. We discuss these problems next.

Geometric complications. In deviated and horizontal wells, heavy pipe and drill collar weight implies eccentric positioning within the borehole, as shown in (a) of Fig. 1, leading to difficulties in geometric description and solution. High eccentricities are often accompanied by non-symmetrical washouts, thick and irregularly formed cuttings beds, and possibly, fracture indentations. Early in petroleum engineering, the notion of a simple "mean hydraulic radius" permitting representation as an equivalent circular pipe flow, as depicted in (b) of Fig. 1, was widely employed; this approach, however, was not useful since what is meant by "mean" is not obvious and certainly not generally applicable from one situation to the next. Later "slot flow" models "unwrapped" the eccentric annulus, with the result as

illustrated in (c) of Fig. 1, and then, further discretized the resulting slot into local parallel plate elements, each of which is approximately modeled by simple solutions for fluid flow between ideal parallel plates. While somewhat reasonable, this approach applied strictly to very narrow annuli, but even then, curvature terms in the general governing momentum equations are always neglected. Thus, inertial effects are never properly modeled even in the limit of very narrow elements.

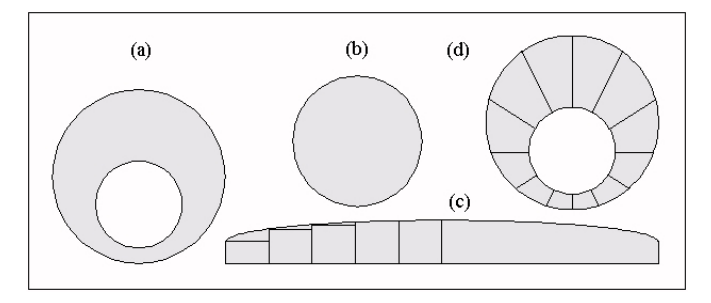


Fig. 1 – Idealizations commonly used to represent eccentric borehole annuli.

Improvements to slot flow models are provided by "pie slice" formulations, idealized in (d) of Fig. 1, in which eccentric annuli are represented by "pie slices" of varying size and included angle having the pipe center as a virtual origin. The solution for each slice is taken from the numerical solution for a concentric annular problem with a closely matched radius. In this approach, pie slices ranging from small to large are used. However, it is clear from the sketch that perfect geometric matching of the borehole boundary is never completely achieved, so that adequate modeling of curvature effects is approximate at best. Moreover, the concentric solutions used are numerical in the case of yield stress fluids and awkward in implementation. More recently, authors have used "bipolar coordinates" to represent eccentric circles, and while these provide useful host formulations for zero-yield-stress fluids, the algebra required to represent even the simplest non-Newtonian flow problems is overwhelming compared to the methods introduced later. The mapping method used in the present paper, it turns out, provides superior modeling capabilities in that the complete momentum equation for any rheology and annular geometry can be solved exactly. The new approach is less intensive numerically and easily describes realistic cuttings beds, washouts and fracture indentations.

Geometric difficulties, however, are much more than what meets the eye. When yield stress fluids flow, "plug regimes" that move as solid bodies are always present in flow domains below a given yield stress. When slot flow or pie slice models are used to simplify the solution process, "plug rings" are always obtained by virtue of the adhoc recipes described above. This is physically incorrect in most operational situations characterized by high eccentricity. For example, one would expect a large, isolated, almost circular plug element at the wide side of (a) of Fig. 1 and perhaps in a

narrow strip at the bottom, but a flow containing such a solid plug would be ruled out by both solution methods. Until recently, of course, exact solutions for (a) of Fig. 1 with yield stress fluids, e.g., Bingham plastics and Herschel-Bulkley models, were impossible anyway for one important reason – theoretically, the size and shape of the plug zone are unknown in problems without azimuthal symmetry, and without knowledge of these internal boundary properties, a complete flow solution could not be obtained. This paper addresses and solves this problem in its complete generality.

Mathematical difficulties. Ideally, one would represent the details of highly eccentric annular domains exactly and in their entirety using boundary-conforming, curvilinear meshes, to which the governing equations of motion would be written, solved, and post-processed for relevant engineering information. However, this is often numerically difficult because there are as many distinct partial differential equation formulations as there are fluid rheologies, e.g., the equations for Newtonian, power law, Bingham plastic and Herschel-Bulkley fluids are very different, each with its own convergence, stability and physical properties. because the equations are generally nonlinear, solutions must be obtained by iterative means. In fact, iterative solutions solving complicated grid generation equations must be followed by iterative solutions to produce the required flowfields on the resulting meshes. These difficulties are compounded, typically, by user inexperience in computational grid generation and numerical analysis. Even when solutions to underlying velocity fields are available, post-processed field solutions for shear rate, viscous stress, apparent viscosity, and so on, need to be automated and rapidly displayed in order to be useful in real-time applications. This requirement is particularly relevant in ultra-deepwater applications since fast and accurate pressure solutions are required to navigate the narrow window between formation fracture and disastrous blowout. These problems are all addressed in the software development program.

User interface considerations. Assuming that both geometric and mathematical issues can be addressed satisfactorily, human factors issues relating to software usage become all-important especially in anticipated applications to managed pressure drilling in ultra-deepwater drilling and holecleaning at high deviation angles. Physical formulations must be mathematically rigorous, numerical solutions must be detailed and pertinent to the annular geometry at hand, and complete field solutions for all engineering properties must be achievable in a manner that is completely transparent to typical engineering users with undergraduate degrees — and, even better, to field technicians with minimal modeling experience or mathematical training. This requires fully automatic grid generation, nonlinear equation setup and stable matrix inversion.

The user interface must be designed with rigsite workflows in mind. Importantly, accuracy and speed, that is, "desktop speed" from problem definition to automated color displays, go hand-in-hand, because of demands imposed by narrow margins between pore-pressure and fracture-pressure

gradient profiles in modern offshore applications. All of the above considerations, again, accurate geometric modeling, rigorous mathematical formulation and solution, and fast, user-friendly, graphically-oriented software implementation, render the general annular flow modeling problem extremely challenging. We now address each of the foregoing issues and explain how the solutions satisfactorily address these needs.

Exact Geometric and Mathematical Formulation

Boundary-conforming, curvilinear meshes. Coordinate systems "natural" to engineering problems play vital roles in facilitating efficient and accurate computational solutions. For example, circular coordinates are natural to circular wells producing from infinite reservoirs, while rectangular systems are ideal for problems solving, say, temperature distributions on rectangular plates. By the same token, a mesh system suitable for eccentric annular geometries would have inside coordinate lines that coincide with circular or square drill collars with stabilizers, while outside lines would conform to irregular borehole walls with their cuttings beds, washouts and fracture indentations. A second set of coordinate lines might be constructed orthogonally to the first, although this is not necessary if all terms in the resulting transformed governing equations are retained. By contrast, it is clear that rectangular (x,y) or circular (r,θ) coordinates are less than satisfactory for accurate geometric description of general annuli.

In natural "boundary-conforming, curvilinear coordinates," here denoted by (ξ,η) , boundary conditions would be easily specified. For example, the no-slip velocity condition for stationary surfaces, say, at pipe and borehole surfaces, is simply described by "u=0" along horizontal grid lines $\xi=\xi_{\text{pipe}}$ and $\xi=\xi_{\text{borehole}}$ where the subscripted numbers are constants. By contrast, the formulation in rectangular coordinates would require u=0 applied along cumbersome curves, e.g., $u\{x,f(x)\}=0$ where y=f(x) represents internal and external contours.

The objective behind grid generation is a set of transformations $\xi(x,y)$ and $\eta(x,y)$ that enable simple boundary condition implementation, so that a complicated physical region, here the eccentric borehole annulus, becomes a simple rectangular one in a computational domain, where the solution of the mathematical problem is undertaken. Once the mapping transforms are available, the governing equation itself must be expressed in the new coordinates. For example, the partial differential equation for steady-state, two-dimensional, Newtonian fluid flow is the well known $u_{xx}+u_{yy}=-\mu^{-1}\ \partial P/\partial z$ where μ and $\partial P/\partial z$ represent viscosity and applied pressure gradient. Although this appears in rectangular coordinates, the equation applies to all annular geometries.

The conversion process itself is straightforward. Suppose we wish to express a function u(x,y) in terms of convenient independent variables ξ and η . If the transformations $x = x(\xi, \eta)$ and $y = y(\xi, \eta)$ are available, direct substitution allows us to rewrite u(x,y) in the form $u(x,y) = U(\xi, \eta)$, where the functional relation $U(\xi, \eta)$ between ξ and

 η is generally different from the relation u(x,y) connecting x and y. Derivatives of u(x,y) with respect to x and y are easily related to derivatives of $U(\xi,\eta)$ taken with respect to ξ and $\eta.$ For example, it is easily shown that $U_\xi=u_xx_\xi+u_y\,y_\xi$ and $U_\eta=u_xx_\eta+u_y\,y_\eta$ for the first derivatives, with obvious extensions to second derivatives obtained using the chain rule of calculus. In general fluid-dynamical problems, the resulting equation for $U(\xi,\eta)$ is typically more complicated than that for u(x,y). The computational benefit, however, is accurate and noise-free implementation of boundary conditions, not to mention the use of much fewer grid points for the same level of physical resolution. Calculated solutions are displayed in physical space with the assistance of custom color plotting routines.

Many commercial simulators calculate velocities and other flow properties directly using rectangular (x,y) grids. We emphasize that x-y coordinate lines do not conform to the irregular curves defining near and farfield boundaries; also, high grid densities imposed, say at the bottom of an eccentric annulus, would require similarly high densities far away where detailed resolution is unnecessary. This results in large, inefficient computing domains containing dead flow and extremely large matrices. In addition, "choppy" meshes lead to noise, inaccuracy and instability. Other simulators, particularly general purpose codes used in computational fluid dynamics (CFD), do support automatic and efficient "finite element" or "finite volume" gridding. However, they are not portable in the sense that special licenses must be purchased for users, thus incurring significant costs. But more importantly, they run proprietary, high-overhead "canned" routines that cannot be adapted to new mathematical models (such as the novel yield stress formulation introduced below) and cannot be "tuned" to run optimally. Also, they offer inflexible output formats that are not easily integrated with custom designed graphics and user interface software. In this paper, the objective is a fast, flexible and accurate solution procedure that can be installed on all operating systems at minimal cost.

We conceptually describe the grid generation process in this paper. Details are offered in the principal author's books on drilling and reservoir engineering, e.g., see Chin (1992, 2001, 2002). We reiterate the basic ideas here because they are essential to understanding the solution approach and its topological advantages. Rather than dealing directly with $\xi = \xi(x,y)$ and $\eta = \eta(x,y)$, we equivalently consider the inverse functions $x = x(\xi,\eta)$ and $y = y(\xi,\eta)$ satisfying *nonlinear* coupled partial differential equations, which are derived in the form

$$\begin{split} &(x_{\eta}^{\ 2}+y_{\eta}^{\ 2})\ x_{\xi\xi}\ -2\ (x_{\xi}x_{\eta}+y_{\xi}y_{\eta})\ x_{\xi\eta}\ +(x_{\xi}^{\ 2}+y_{\xi}^{\ 2})\ x_{\eta\eta}\ =0 \quad (1)\\ &(x_{\eta}^{\ 2}+y_{\eta}^{\ 2})\ y_{\xi\xi}\ -2\ (x_{\xi}x_{\eta}+y_{\xi}y_{\eta})\ y_{\xi\eta}\ +(x_{\xi}^{\ 2}+y_{\xi}^{\ 2})\ y_{\eta\eta}\ =0 \quad (2) \end{split}$$

where ξ and η are now independent (as opposed to dependent) variables. We aim to map the irregular flow domain of Fig. 2a into the simple rectangular computational domain of Fig. 2b where B_1 and B_2 are physically insignificant "branch cuts" where single-valued solution constraints are enforced.

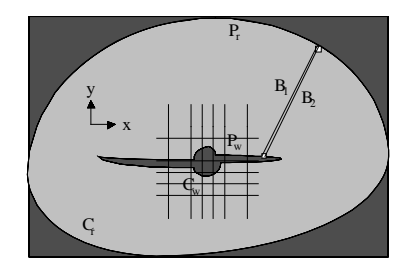


Fig. 2a – Irregular physical domain with inefficient rectangular meshes

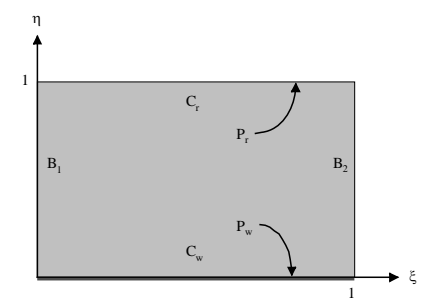


Fig. 2b – Irregular domain mapped to rectangular computational space.

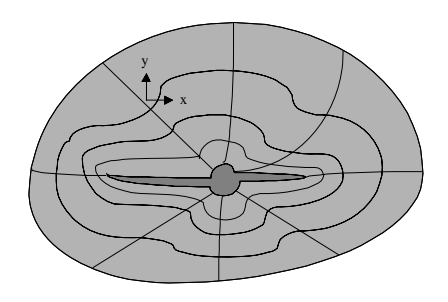


Fig. 2c - Physical domain in boundary-conforming coordinates.

How are the foregoing equations used to create numerical mappings? Suppose that contour C_W in Fig. 2a is to map into $\eta=0$ of Fig. 2b. The user first discretizes C_W in Fig. 2a by penciling along it a sequence of dots chosen to represent the curve. If these are selected in an orderly, say, clockwise fashion, they define the direction in which ξ increases. Along $\eta=0,$ values of x and y are known (e.g., from measurement on graph paper) as functions of ξ . Similarly, x and y values along C_r are known as functions of ξ on $\eta=1$ of Fig. 2b. These provide the boundary conditions for Eqs. 1 and 2, which are augmented by single-valuedness constraints at arbitrarily chosen branch cuts B_1 and B_2 . It is clear that this process is easily automated by computer.

Conventionally, in grid generation, Eqs. 1 and 2 are discretized by finite differences and solved by point or line relaxation, starting with guesses for the dependent variables x and y. The problem is linearized by approximating all nonlinear coefficients using values from earlier iterations. Typically, several updates to Eq. 1 are taken, followed by updates to Eq. 2, with this cycling process, often unstable,

repeated continuously until convergence. Variations of the approach are known, with 100×100 mesh systems in the ξ - η plane requiring minutes of computing time. Once $x=x(\xi,\eta)$ and $y=y(\xi,\eta)$ are solved and tabulated as functions of ξ and $\eta,$ physical coordinates are generated. First, η is fixed; for each node ξ along this $\eta,$ computed values of (x,y) pairs are successively plotted in the x-y plane to produce the required closed contour. This procedure is repeated for all values of $\eta,$ until the entire family of closed curves is obtained, with limit values $\eta=0$ and $\eta=1$ again describing C_w and $C_r.$ Orthogonals are constructed by repeating the procedure, with η and ξ roles reversed.

This process provides the curvilinear mapping only. The equation describing the physics (e.g., the Navier-Stokes equation for Newtonian flow or the general rheological equations for non-Newtonian fluids) must be transformed into (ξ,η) coordinates and solved. In general, the transformed governing equation, which is algebraically more complicated, must be solved, and this procedure introduces its own complications and numerical challenges. "simplification," however, lies not in the transformed equation, which now contains mixed derivatives and variable coefficients, but in the computational domain itself, because this domain takes on a rectangular form amenable to simple, noise-free numerical solution, requiring significantly fewer nodal points for high resolution physical definition.

Again, existing solution methods solving $x(\xi,\eta)$ and $y(\xi,\eta)$ stagger the solutions for Eqs. 1 and 2. For example, crude solutions are used to initialize the coefficients of Eq. 1, and improvements to $x(\xi,\eta)$ are obtained. These are used to evaluate the coefficients of Eq. 2, in order to obtain an improved $y(\xi,\eta)$; then, attention turns to Eq. 1 again, and so on, until convergence is achieved. Various over-relaxation means are used to implement these iterations, e.g., point SOR, line SLOR, line SOR with explicit damping, alternating-direction-implicit, and multigrid, with varying degrees of success. Often these schemes diverge computationally. In any event, the staggering used introduces different artificial time levels while iterating. Classic numerical analysis, however, suggests that faster convergence and improved stability are possible by reducing the number of time levels.

A new approach to rapidly solve the nonlinear coupled grid generation equations was proposed by the principal author a decade ago and is based on a very simple idea. This idea has since been validated in numerous applications. Consider first $z_{\xi\xi}+z_{\eta\eta}=0,$ for which $z_{i,j}\approx(z_{i-1,j}+z_{i+1,j}+z_{i,j-1}+z_{i,j+1})/4$ holds on constant grid systems (this is easily derived using standard finite difference formulas). This well-known averaging law motivates the $\mathit{recursion formula}\ z_{i,j}^n=(z_{i-1,j}^{n-1}+z_{i+1,j}^{n-1}+z_{i,j-1}^{n-1}+z_{i,j+1}^{n-1})/4$ often used to illustrate and develop multilevel iterative solutions; an approximate, and even trivial solution, can be used to initialize the calculations, and nonzero solutions are always produced from nonzero boundary conditions.

But the well-known Gauss-Seidel method is fastest: as soon as a new value of $z_{i,j}$ is calculated, its previous value is

discarded and overwritten by the new value. This speed is accompanied by low memory requirements, since there is no need to store both n and n-1 level solutions: only a single array, $z_{i,j}$ itself, is required in programming. The approach to Eqs. 1 and 2 was motivated by the following idea. Rather than solving for $x(\xi,\eta)$ and $y(\xi,\eta)$ in a staggered, leap-frog manner, is it possible to *simultaneously* update x and y in a similar once-only manner? Are convergence rates significantly increased? What formalism permits us to solve in Gauss-Seidel fashion? What are the programming implications?

Complex variables are used often in harmonic analysis problems; for example, the real and imaginary parts of an analytical function f(z), where z=x+i y, provide solutions satisfying Laplace's equation. Here we use complex analysis differently. We *define* a dependent variable z by $z(\xi,\eta)=x(\xi,\eta)+i$ y(ξ,η), and then add Eq. 1 plus i times Eq. 2, in order to obtain the net result $(x_\eta^2+y_\eta^2)$ z $\xi\xi-2$ $(x_\xi x_\eta+y_\xi y_\eta)$ z $\xi\eta+(x_\xi^2+y_\xi^2)$ z $\eta\eta=0$. Now, the complex conjugate of z is $z'(\xi,\eta)=x(\xi,\eta)-i$ y(ξ,η), from which we find that $x=(z+z^*)/2$ and y=-i (z - z^*)/2. Substitution produces the simple and equivalent one-equation result

$$(z_{\eta} z_{\eta}^{*}) z_{\xi\xi} - (z_{\xi} z_{\eta}^{*} + z_{\xi}^{*} z_{\eta}) z_{\xi\eta} + (z_{\xi} z_{\xi}^{*}) z_{\eta\eta} = 0$$
 (3)

This form yields significant advantages. First, when z is declared as a complex variable in a Fortran program, Eq. 3 represents, for all practical purposes, a single equation in $z(\xi,\eta)$. There is no need to leap-frog between x and y solutions now, since a single formula analogous to the classical model $z_{i,j}=(z_{i-1,j}+z_{i+1,j}+z_{i,j-1}+z_{i,j+1})/4$ is easily written for the $z_{i,j}$ using Eq. 3 as the host equation. Because both x and y are simultaneously resident in computer memory, the extra time level present in staggered schemes is completely eliminated, as in the Gauss-Seidel method. In thousands of test simulations conducted using point and line relaxation, convergence times are shorter by orders of magnitude relative to those obtained for cyclic solution between $x(\xi,\eta)$ and $y(\xi,\eta)$. Convergence appears to be unconditional, monotonic and stable. Because Eq. 3 is nonlinear, von Neumann tests for exponential stability and traditional estimates for convergence rate do not apply, but the evidence for stability and convergence, while empirical, remains very strong and convincing since we have always computed useful grids in all test runs.

Iterative solution of nonlinear partial differential equations. Earlier we noted that $u_{xx} + u_{yy} = - \mu^{-1} \partial P/\partial z$ applies to steady, two-dimensional, single-phase Newtonian flows for borehole annuli having the most complicated shapes; unfortunately, practical solutions cannot be accurately obtained in (x,y) coordinates. Here, μ is a constant viscosity and $\partial P/\partial z$ is the applied pressure gradient in the z direction assumed to be known. This is the so-called Poisson equation in mathematics, and students who have undertaken its study realize that, despite the apparent simplicity offered by few terms and complete linearity, useful solutions to the classical model are nonetheless difficult to obtain. When the underlying fluid is nonlinear, this equation is replaced by Eq.

4, which is vastly more complicated, that is,

$$\partial (N \partial u/\partial y)/\partial y + \partial (N \partial u/\partial x)/\partial x = \partial P/\partial z$$
 (4)

where N now represents the "apparent viscosity" function. This apparent viscosity is not constant, but a function of local shear rates whose mathematical form depends on the particular rheology assumed. For example, in the case of power law fluids modeled by an exponent "n" and a consistency factor "K," N takes the form $N = K [(\partial u/\partial y)^2 + (\partial u/\partial x)^2]^{(n-1)/2}$. Even without solving the problem, it is clear that, since $\partial u/\partial x$ and $\partial u/\partial y$ depend on the (unknown) solution itself, any resulting apparent viscosity must vary locally within the flow domain and depend on both geometric details and flow rate. Detailed computed solutions for annular flows are presented in Chin (1992, 2001) where approximate approaches to plug flow modeling are used.

Because Eq. 4 is now strongly nonlinear, the solution process at its very heart must remain nonlinear. This implies that one cannot use simpler Newtonian solutions as leading approximations and focus on higher order improvements to them. The basic solution method must retain a fully nonlinear character in order that well known nonlinear relationships between pressure gradient and volume flow rate evolve as part of an iterative computational process. As if this alone were not complicated enough, we emphasize that it is the reexpression of Eq. 4 in general (ξ,η) curvilinear coordinates, not in simple (x,y) coordinates, that must be solved, and that these coordinates and their metrics are only available numerically.

The transformed equation now contains additional terms as well as nonlinear coefficients that depend on the mapping. Direct solutions are not numerically possible, but exact solutions can be obtained iteratively. In fact, finite difference methods are used; the solutions are obtained line-by-line using so-called "successive line over relaxation" (SLOR) schemes written in the curvilinear coordinates. These iterative solutions are initialized by "close" analytical or numerical solutions: the closer the initial guess, the more rapid the convergence. For typical problems, the efficient schemes devised will produce a usable curvilinear grid in approximately one second of computing time, while the solution of the transformed momentum equation (when pressure gradient is specified) may require two-to-three seconds. Again, detailed discussions and computed solutions for power law and simple plug flows in highly eccentric annuli, with practical applications, are given in Chin (1992, 2001). The approximate plug flow methods developed in these early researches are now obsolete and are replaced by the following exact approach for yield stress description and modeling.

Yield stress, plug zone size and shape modeling. In fluid flows where yield stresses exist, "plug zones" are to be found. These plugs move as solid bodies within the flowing system. For pipes with circular cross-sections and for concentric annuli, it is possible to derive exact analytical solutions for plug zone size and shape for Bingham plastics

(general solutions have, in fact, been derived for both geometries assuming Herschel-Bulkley fluids, and will be presented separately). For circular pipes, the cross-sectional plug is simply a circle; for concentric annuli, of course, the plug is a concentric ring.

The appearance of solid plugs within moving streams results from the rheological model used by mathematicians to idealize the physics. If we now denote the shear rate for the flow by $\Gamma = [\ (\partial u/\partial y)^2 + (\partial u/\partial x)^2\]^{1/2}$, this idealization can be written formally as

$$N = k \Gamma^{n-1} + S_{yield}/\Gamma \text{ if } \{1/2 \text{ trace } (\underline{\underline{\mathbf{S}}} \bullet \underline{\underline{\mathbf{S}}})\}^{1/2} > \tau_0$$

$$\underline{\mathbf{D}} = 0 \text{ if } \{1/2 \text{ trace } (\underline{\mathbf{S}} \bullet \underline{\mathbf{S}})\}^{1/2} < \tau_0$$
 (5)

where the general extra stress tensor is denoted by $\underline{\mathbf{S}}$ and the deformation tensor is given by $\underline{\mathbf{D}}$. Here, τ_0 is the so-called "yield stress." The discontinuous "if, then" character behind Eq. 5 is responsible for the sudden transition from shear flow to plug flow commonly quoted. As noted, for flows with azimuthal symmetry, that is, circular pipes and concentric annuli, exact, rigorous mathematical solutions are in fact possible.

For non-circular ducts and eccentric annuli, which describe a large number of practical engineering problems, it has not been possible to characterize plug zone size and shape, even approximately. Thus, the most significant petroleum engineering flow problems important to both drilling and cementing cannot be modeled at all, let alone accurately. In order to remedy this situation, we observe that the discontinuity offered in Eq. 5 is really an artificial one, introduced for, of all reasons, "simplicity." This unfortunately leads to the solution difficulties noted. In reality, practical engineering flows do not suddenly turn from shear to plug flow; the transition may be rapid, but it will occur continuously over finite measurable distances. We therefore turn to more realistic rheological models which apply continuously throughout the entire problem domain, and which, if the underlying flow parameters permit, lead to plug zones naturally during the solution process.

The conventional Herschel-Bulkley viscoplastic model, which includes Bingham plastics as a special limit when the exponent "n" is unity, requires that $\tau=\tau_0+K(d\gamma/dt)^n$, if $\tau>\tau_0$ and $d\gamma/dt=0$ otherwise. Here τ is the shear stress, τ_0 is the yield stress, K is the consistency factor, n is the exponent, and $d\gamma/dt$ is the shear rate. As explained, this model is far from perfect. For example, both Herschel-Bulkley and Bingham plastic models predict infinite viscosities in the limit of vanishing shear rate, a fact that often leads to numerical instabilities. In addition, the behavior is not compatible with conservation laws that govern many complex flows.

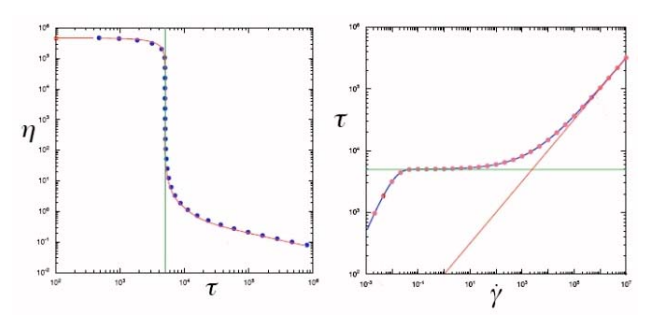


Fig. 3 - Extended Herschel-Bulkley law.

An alternative to the standard Herschel-Bulkley model is the use of continuous functions which apply to sheared regimes, and in addition, through and into the plug zone. One such example model is suggested by Souza, Mendez and Dutra (2004), that is, $\tau = \{1 - \exp(-\eta_0 \ d\gamma/dt \ /\tau_0)\}\{\tau_0 + K \ (d\gamma/dt)^n\}$, which would apply *everywhere* in the problem domain. The corresponding apparent viscosity N, for numerical implementation in Eq. 4, is denoted by

$$\begin{split} \eta &= \tau \, / (d\gamma \, / dt) \\ &= \{1 - exp(-\eta_0 \, d\gamma / dt \, / \tau_0)\} \{\tau_0 / (d\gamma / dt) + K \, (d\gamma / dt)^{n-1}\} \end{split} \tag{6}$$

The "apparent viscosity vs shear stress" and "shear stress vs shear rate" diagrams, from Souza et al, are duplicated in Fig. 3. What are the physical consequences of this model? Eq. 6, in fact, represents an "extended Herschel-Bulkley" model in the following sense. For infinite shear rates, one would recover $\tau = \tau_0 + K (d\gamma/dt)^n$. But for low shear rates, a simple Taylor expansion leads to $\eta \approx \{\eta_0(d\gamma/dt)/\tau_0\}\{\tau_0/(d\gamma/dt) + K$ $(dy/dt)^{n-1}$ $\approx \eta_0$ where it is clear now that η_0 represents a very high viscosity for the plug zone. The use of Eq. 6 in numerical algorithms simplifies both formulation and coding since internal boundaries and plug domains do not need to be determined as part of the solution. A single constitutive law (as opposed to the use of two relationships in Eq. 5) applies everywhere, thus simplifying computational logic; moreover, the continuous function assumed also possesses continuous derivatives everywhere and allows the use of standard difference formulas. Cumbersome numerical matching across internal boundaries is completely avoided. In a practical computer program, the plug zone viscosity might be assumed, for example, as 1,000 cp. In fact, we choose high values of η_0 which would additionally stabilize the numerical integration schemes used. This strategy is applied throughout this work, both to the iterative relaxation schemes for steady-state problems and to the transient integration schemes for more complicated formulations. This new approach was first discussed in Chin and Zhuang (2010) for steady flows and has since been incorporated in the fully transient annular flow modeling approaches.

Borehole axis radius of curvature. Borehole axis curvature is important to ultra-deepwater drilling, especially in short and medium radius turning applications. Several aspects of cuttings transport and debris removal are not completely understood insofar as centrifugal effects are concerned and a

study of curvature effects contributes to an understanding of their influence on stress fields. Also, bends in pipelines and annuli are interesting because they are associated with losses; that is, to maintain a prescribed volume flow rate, a greater pressure drop is required in pipes with bends than those without. This is true because the viscous stresses acting along pipe walls are higher. The modeling of borehole axis curvature effects for problems involving noncircular ducts and highly eccentric annuli containing non-Newtonian fluids was first addressed in Chin (2001), where detailed derivations, equations and computed examples are given. Essentially, it is shown how, by replacing " $1/\mu$ $\partial P/\partial z$ " with an inertially corrected " $1/\mu \partial P/\partial z - 1/R \partial u/\partial r + u/R^2$ " where R is the radius of curvature, the effective pressure gradient accounting for centrifugal effects is properly and stably modeled. This model is incorporated into Eq. 4 and a radius of curvature entry appears in the software menu in Fig. 4a at the bottom left.

Steady and Transient Formulations: User Interface and Physical Modeling Capabilities

Simulators for two-dimensional steady and transient flow are described in this paper, applicable to single-phase, Herschel-Bulkley fluids, which may also be operated in Newtonian, power law and Bingham plastic modes. For Bingham plastic and Herschel-Bulkley fluids, the generalized rheological approach is used and plug zone sizes and shapes are determined automatically whatever the eccentric annular The intuitive user interface shown in Fig. 4a geometry. requires only an elementary understanding of engineering vocabulary and the simulator may be operated with minimal training. Annular geometry is defined by entering center coordinates and radii in the upper left menu. Clicking 'Show Annulus' provides an instantaneous display of the geometry assumed, plus a typical curvilinear grid, e.g., as illustrated in Fig. 4b, whose mesh density may be coarsened or refined at In addition, online editing utilities allow the baseline eccentric circles to be edited for washout, cuttings bed or fracture modification effects.

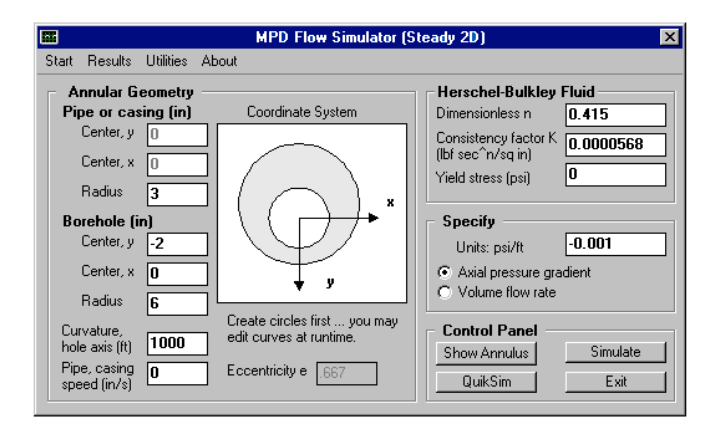


Fig. 4a - Steady flow user interface.

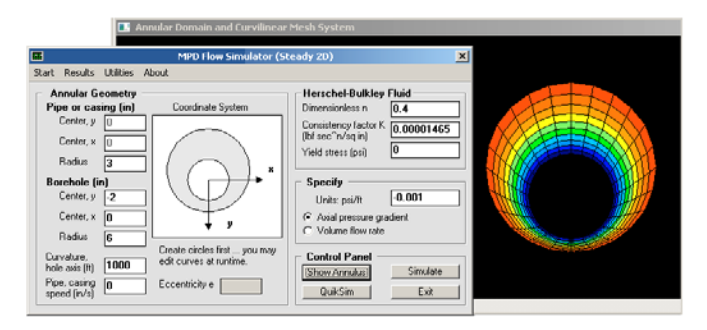


Fig. 4b – Quick annular geometry and curvilinear grid display mode.

Rheological parameters for the general Herschel-Bulkley fluid are entered into the input boxes at the upper right of Fig. 4a. Four model are possible by choosing the values of n, K and τ_0 appropriately. Newtonian fluids require n=1 and $\tau_0=0$, while power law fluids allow general n with vanishing τ_0 . On the other hand, Bingham plastics require n=1 and non-vanishing τ_0 , while all three parameters may be generally assumed in the case of Herschel-Bulkley fluids. Fig. 4c also shows two utilities for n and K determination in the case of power law fluids, that is, assuming Fann dial readings or viscosity and shear rate data are available.

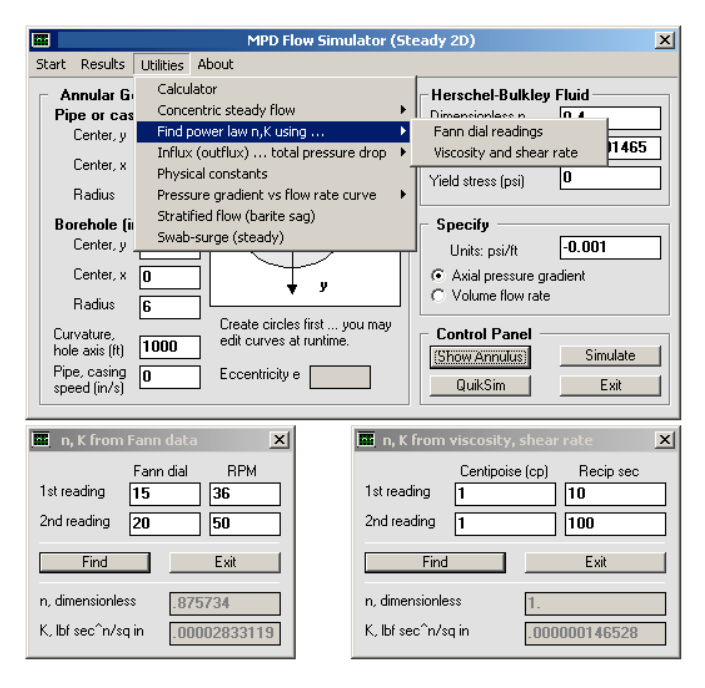


Fig. 4c - Determining n and K for power law fluids.

It is clear from Figs. 4a – 4c that several important auxiliary capabilities have been built into the overall algorithm. First, the axis of the borehole need not be straight; it may be curved, with any constant value for radius of curvature, to model short, medium and large radius turning of the borehole in offshore applications. This properly accounts for centrifugal effects which will affect the relationship between pressure gradient and volume flow rate.

Second, the drillpipe may move in either direction relative to the borehole, that is, constant speed translational motion is permitted. In the simplest application, the drillstring penetrates the formation, moves relative to the borehole at constant positive or negative speed, and induces a purely twodimensional flow everywhere; the value of this speed is entered into the bottom left input box of Fig. 4a. This capability also supports steady-state swab-surge analysis, with the mudpumps turned off or on and continuously running, as will be illustrated in examples later. A simple 'Worksheet' is loaded by clicking 'Swab-surge (steady)' in Fig. 4c, which prompts the user for tripping mode and speed. The positive or negative induced volume flow rate is calculated and added to the flow rate specified at the mud pump. Two calculation modes described in the next paragraph was developed for swab-surge and other drilling and cementing applications.

The option boxes immediately above the 'Control Panel' in Fig. 4a show how two computational modes are supported. In the first, the applied axial pressure gradient is specified and volume flow rate (together with detailed field solutions for all physical properties) is calculated. In the second, volume flow rate is specified and pressure gradient (together with all field properties again) is determined iteratively. The algorithm involves some subtlety because, as will be described in the application for swab-surge, the directions for drillpipe motion and net volume flow rate need not be correlated. For the "flow rate specified" mode, an initial pressure gradient is assumed for which a test rate is calculated and compared against the target rate; if the results do not satisfy a tolerance of 1%, a half-step correction procedure is applied to the test gradient and the calculations are repeated to convergence. Typically, the "pressure gradient specified" mode requires 2-3 seconds or less for a complete solution, while the "flow rate specified" mode may require up to ten seconds.

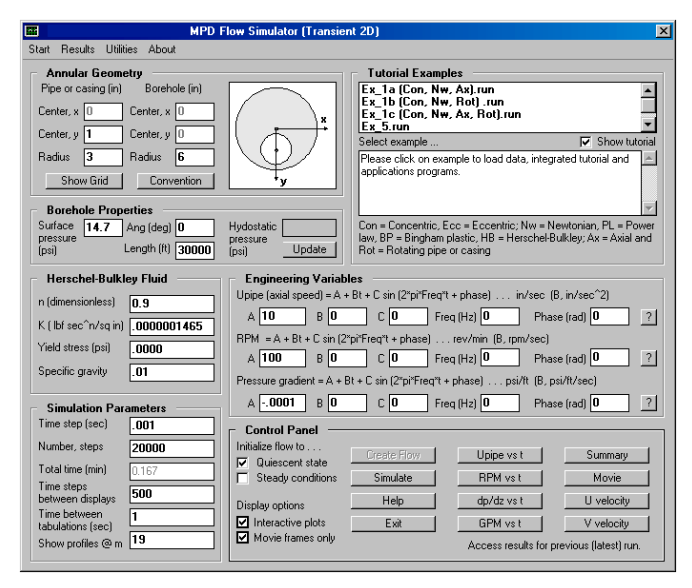


Fig. 4d - Transient flow user interface.

The foregoing remarks, focusing on the screen shot in Fig. 4a, apply to the steady flow simulator. The corresponding user interface for transient incompressible flow is shown in Fig. 4d. Now, instead of Eq. 4, fully unsteady effects are computed from its transient extension, but rewritten in custom curvilinear coordinates applicable to the particular geometry under consideration. The above menu contains similar geometry and rheology definition modules, however, general. coupled, transient functions for pipe or casing axial reciprocation, inner circle rotation and pressure gradient are permitted. Additional input boxes for time step selection to facilitate numerical time integration are shown. Importantly, a database of prior runs is offered for user convenience and education. Clicking on a named entry at the top right of Fig. 4d automatically fills in all relevant input boxes and launches any sub-applications programs that are required. Users may edit numerical values and re-run any simulations available in the database. Also, all graphical capabilities described in this paper for steady flow are also available for unsteady flows.

Color displays of engineering properties. In order to make the mathematical models useful, every effort was expended to automate the display of important field quantities using two and three-dimensional color graphics. Use of the presentation tools is completely transparent to the engineer. An 'Install Graphics' button installs all required software quickly in a single pass; in addition, user training in operating the integrated graphical capabilities is not required. On convergence of the solution, a message box (supplemented with speech output and suggestions) summarizes basic pressure gradient and flow rate relationships.

The menu in Fig. 5a indicates that text output and color displays for different physical quantities are available for display. These quantities are post-processed from the velocity solution and made available for important engineering reasons. For example, Chin (1992, 2001) shows that apparent viscosity is vital to evaluating spotting fluid effectiveness in freeing stuck pipe. On the other hand, viscous stress (at the cuttings bed) is important to studying hole cleaning in horizontal and deviated wells, while velocity and viscosity play dominant roles in vertical well cuttings transport.

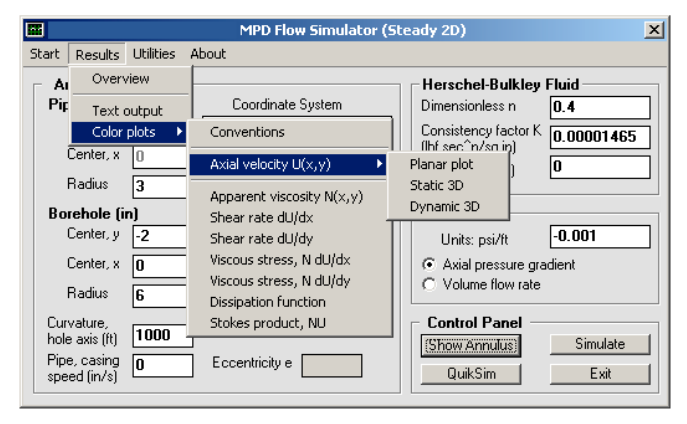


Fig. 5a - Graphical solution display options.

Fig. 5b displays results for axial velocity, apparent viscosity, shear rate, viscous stress, dissipation function and Stokes product in simple "planar plots." For the all-important velocity results, additional displays using three-dimensional color capabilities are offered as indicated in Fig. 5c. These capabilities, which include contour plots and mouse-rotatable perspective displays, are available for all mesh combinations, ranging from coarse to fine, selected by the user at run-time. These tools, plus text output, are useful in supporting detailed report generation.

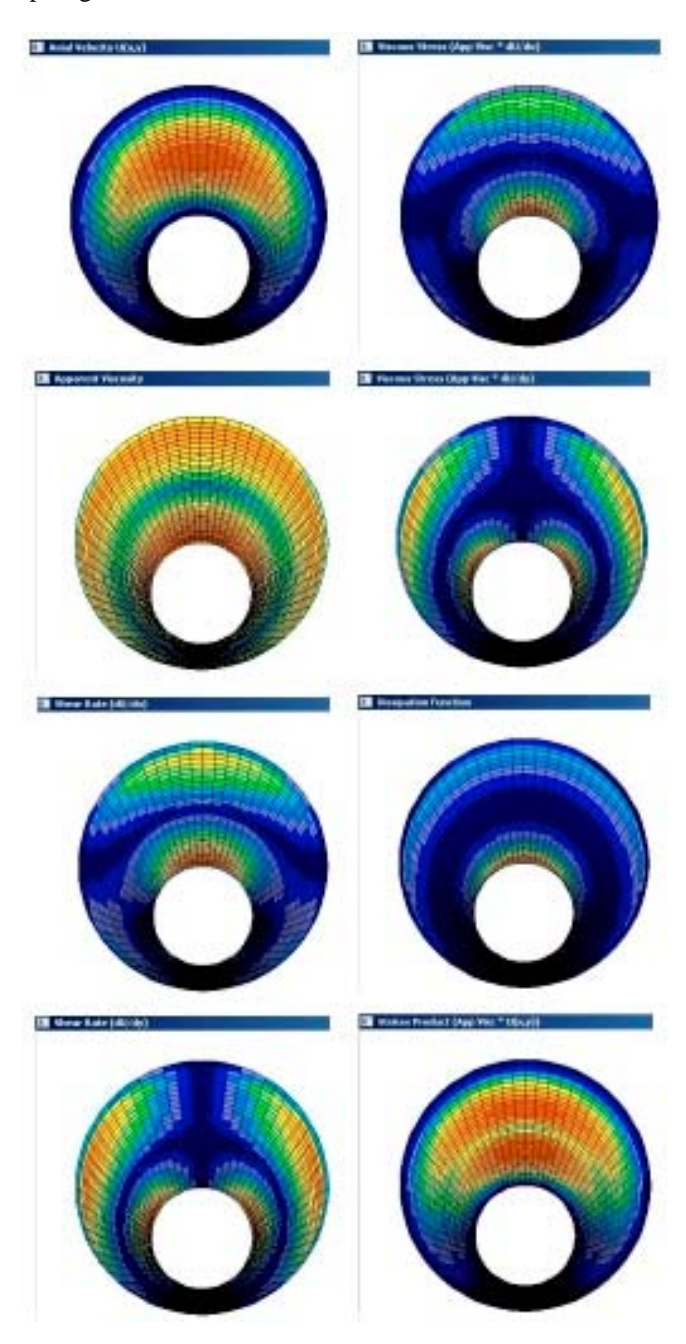


Fig. 5b - Planar color displays of key physical field quantities.

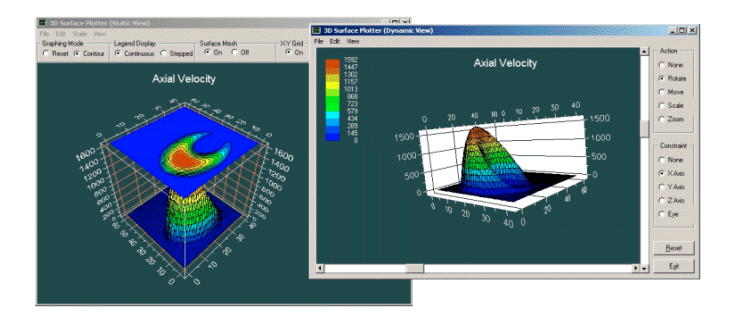


Fig. 5c – Three-dimensional, color displays (contour maps and mouse-rotatable perspective views).

Modeling borehole geometric irregularities. convenience, the main input screen in Fig. 4a accepts offcentered circles only. When center coordinates and radii are entered for inner and outer circles, an information box displays the calculated value for dimensionless eccentricity, to provide a useful reference point for drilling applications. Built-in error checking prevents circle cross-overs. At runtime, both inner and outer circle coordinates may be changed at the user's option. As shown in Fig. 6a below, existing contour coordinates are displayed, which may be modified without restriction. The changes elected for the example shown invoke changes to seven points only, in order to describe a simple washout; this convenient online editing tool can be used to draw washouts, cuttings beds and fracture indentations of any shape. While Fig. 6a provides a simple "planar plot" of velocity, Fig. 6b provides more detailed threedimensional resolution. Interestingly, for the simulation shown, the presence of the washout allows a 30% increase in flow rate for the same pressure gradient. General conclusions are not possible, and appropriate results must be made on a case-by-case basis.

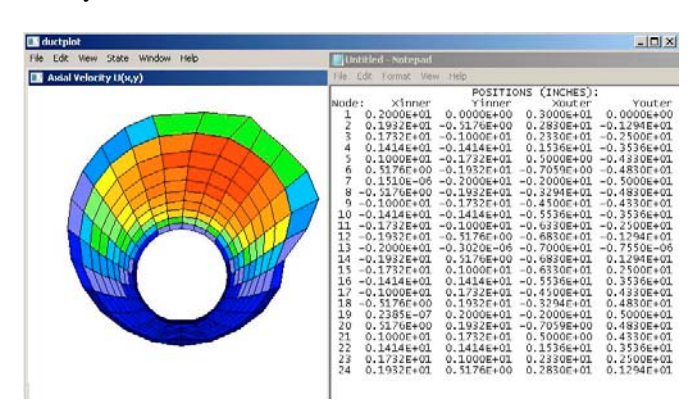


Fig. 6a - Modifying eccentric circle at run-time for washouts.

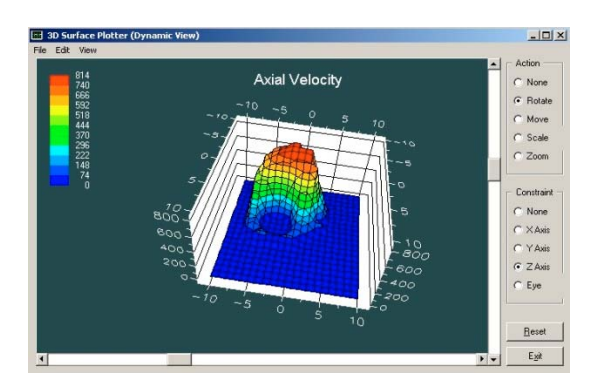


Fig. 6b - Color display of velocity field with washout.

Yield stress modeling. As noted earlier, yield stress modeling in eccentric annuli is important to both drilling and cementing applications. The use of the generalized Herschel-Bulkley constitutive model correctly predicts plug zone size and shape for all geometries. Because a continuous flow model is used, which guides the evolution of a single continuous velocity field, the computational difficulties associated with distinct internal boundaries and infinite viscosities are avoided. The method, we emphasize, will predict realistic plug zones with rapid gradients when they exist, as shown in Fig. 7a.

More interesting results are shown in Fig. 7b, in which plug zones for (1) a stationary pipe, (2) a pipe moving opposite to the direction of net flow, and (3) a pipe moving in the same direction of the main flow, are shown. Such computations are important in swab-surge applications and accurate pressure modeling. Plug zones associated with yield stress, of course, are important to understanding cuttings transport in drilling and fluid mixing in cementing. Again, no special procedures are required on the part of the user, as all dynamical features are computed automatically for both yield stress and non-yield fluids. Computation of plug zone flows requires no additional effort in terms of processing time and memory resources.

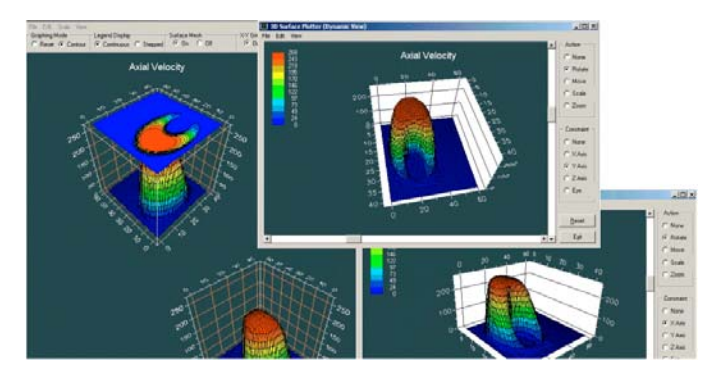


Fig. 7a – Typical velocity results for eccentric annulus with plug flow.

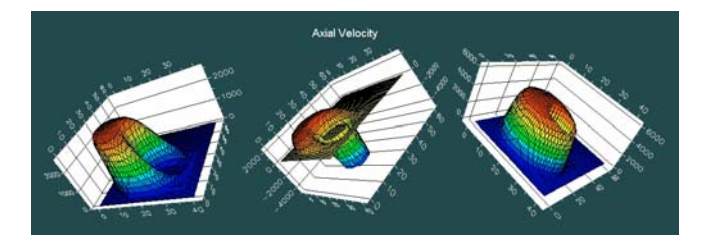


Fig. 7b – Non-Newtonian plug flow velocity profiles with stationary pipe (left), pipe moving opposite to flow (middle), and pipe moving with flow (right).

Swab-Surge Applications

During tripping, drill pipe run rapidly into the borehole may create large "surge" pressures that can lead to lost circulation and formation fracture. On the other hand, when pipe is removed too quickly, large "swab" (or negative surge) pressures may be induced that can lead to kicks and blowouts. Numerous models have been developed for swab-surge applications over the past three decades which are based on different physical assumptions. The earliest models assume steady-state flows in which borehole fluid reacts instantaneously to drillbit movement and develops fully established annular flow profiles. In this paper, we address both steady-state and fully transient models for incompressible non-Newtonian flow.

Recently, "transient models" have become available which are supposedly more realistic for practical application. The literature on transient modeling, however, is wrought with unsubstantiated claims, imprecise terminology, and very likely, fortuitous agreement with data. From a fluid-mechanical perspective, "transient" may include two distinct effects which may act independently or in concert. One can have transient incompressible flow in which the effects of fluid inertia are to be assessed; on the other hand, one might consider water-hammer effects in which the effects of fluid compressibility and acoustic-type pressure waves are important. Of course, both types of transients can co-exist in the borehole, in much the same way that it is possible for a child to shout in a blowing wind.

The literature, unfortunately, does not distinguish between the two types of transients. Reference to the single differential equation often cited shows a crude one-dimensional model that has remained unchanged over the years, that is, one for compressible water-hammer signal propagation. This alone points to what cannot be modeled and the limitations are substantial. For instance, these limitations would include the effects of hole eccentricity, actual rheological effects, and pipe movement relative to the hole, an important consideration in swab-surge applications given that tripping speeds can be comparable to fluid speeds. Computed results usually presented to validate the models neglect these considerations.

The rigorous development of swab-surge models requires a firm foundation based on solid mathematics. Whether the flow is steady, or transient in both of the foregoing senses, accurate hydraulic models that represent

eccentricity, rheology and pipe movement are necessary. Several limits must be considered in the design of "building blocks" for general application. Consider first the conventional surge problem in (a) of Fig. 8 in which pipe is run into the hole and mudpumps are turned off. Displacement of mud beneath the drillbit induces an upward (positive) annular flow. When mud flows while tripping in, as in the case of continuous-circulation managed pressure drilling, the positive annular flow is enhanced, as illustrated in (b) of Fig. 8. In both (a) and (b) of Fig. 8, the net effect is an upward positive flow in which the pipe moves in a direction opposite to the net motion. In this sense, surge flow modeling is simple.

On the other hand, consider the swab flow in (c) of Fig. 8 without pumping. Pulling pipe induces a downward (negative) flow to fill the void left by the retreating drillbit; as shown, the pipe and the net flow always occur in opposite directions. When mud flows, however, two possibilities arise. A very slow pump rate can leave the net flow downward, as shown in (c) of Fig. 8. However, a higher flow rate will have both net flow and pipe motion in the same upward direction, as shown in (d) of Fig. 8, in contrast to (b) of Fig. 8. These observations are, in a sense, obvious, but the four possible flow configurations shown complicate the software logic used in automated swab-surge analysis for "volume flow rate specified" calculations.

In the model, the surface mudpump rate may be zero or positive, while the drillpipe speed may be positive or negative; when the net volume flow rate is specified, the iterative algorithms determine the corresponding axial pressure gradients taking into account the direction of the pipe motion. Typical computing times for this "flow rate specified" mode range from ten to twenty seconds. We emphasize that motion of the pipe relative to borehole walls is an essential part of the formulation that cannot be neglected and that this crucial modeling element is not possible with existing models. In addition, it is mathematically incorrect to obtain swab-surge solutions by subtracting those pressure gradients associated with the mudpump flow alone and the drillbit-induced volume flow alone: as will be seen in one illustrative calculation, the flow rate versus pressure gradient relationship is nonlinear for general non-Newtonian fluid rheologies.

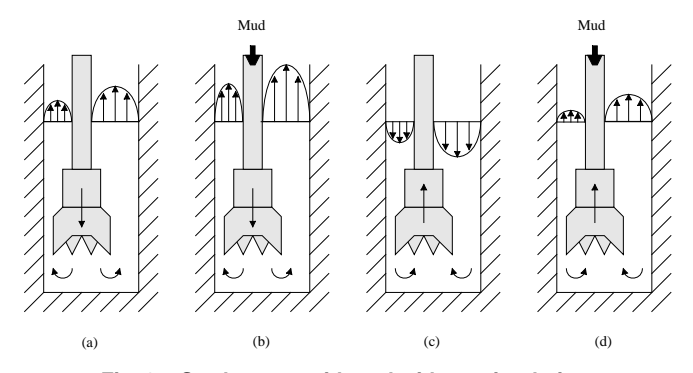
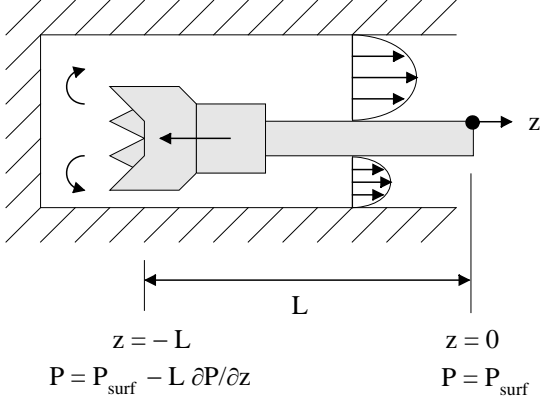


Fig. 8 – Swab-surge with and without circulation.

For the remainder of this paper, we focus on specific swab-surge job planning calculations, through a series of specially designed examples that draw attention to the new capabilities built into the mathematical formulations. We emphasize that all models are developed rigorously from first principles and solved using fast and stable computational methods. Here the objective is a to-the-point demonstration of new methodologies useful for field application.

Example 4-6. Steady-state swab-surge in eccentric annuli for power law fluids with and without circulation (no rotation).

In this example, we discuss applications of the steady-state, non-Newtonian flow simulator to swab and surge analysis for eccentric annuli with and without mud circulation. This problem is important and complementary to new hardware capabilities in managed pressure drilling that allow continuous mud circulation while tripping in and out of the hole. We focus implicitly on long deviated and horizontal wells for which hole eccentricity is very important. Existing models are either concentric, which are inapplicable, or one-dimensional, in which case any details of the annular cross-section are impossible to model. Therefore, this work describes completely new methods that support accurate prediction of pressure distributions in the hole.



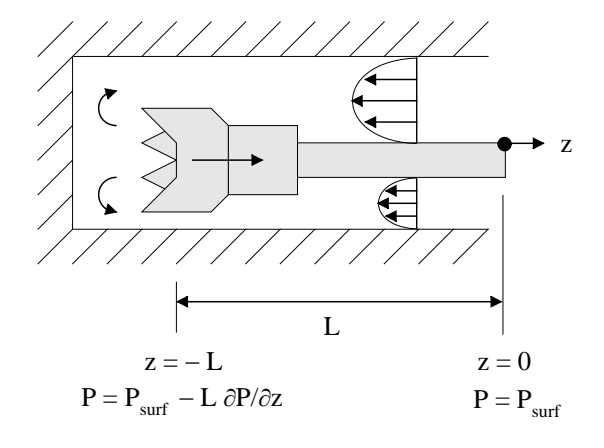


Fig. 4-6a - Coordinate system and conventions.

Basic concepts. The simulator predicts the constant pressure gradient $\partial P/\partial z$ needed to induce a specified volume flow rate Q for any Herschel-Bulkley fluid in an eccentric annulus. By convention, when Q is positive or "flowing to the right," the pressure P falls in the direction of increasing z. Analogously, when Q is negative or "flowing to the left," P increases with increasing z. Let us first consider flows without mud circulation. In the top diagram of Fig. 4-6a, the drillpipe and bit are shown moving toward the bottom of the hole and displacing fluid as it moves to the left. This fluid must then flow to the right as shown and will produce a positive Q. Now, the governing equation for pressure is simply $P = z \partial P/\partial z + constant$. If z = 0 represents the surface where $P = P_{surf}$ is fixed by the driller and z = -L is the bit location with L being the borehole length, then the pressure at the bit is just $P_{bit} = -L \partial P/\partial z + P_{surf}$. Since $\partial P/\partial z < 0$, we have P_{bit} >> P_{surf} which formally shows that in a "surge" situation the bottomhole pressure greatly exceeds that at the surface. Next consider the bottom diagram in Fig. 4-6a. Here we "swab" the drillstring, pulling it out of the hole. To fill the void left by the drillbit, the flow Q must travel toward the left, for which we have $\partial P/\partial z > 0$. Then, $P_{bit} = -L \partial P/\partial z + P_{surf}$ implies that P_{bit} << P_{surf} which formally shows that pressure is greatly reduced at the bit. Increased pressures at the bit are associated with formation invasion and the possibility of fracturing the rock, while decreased pressures may increase the likelihood of blowouts.

The main simulation objective is accurate prediction of P_{bit} as a function of annular geometry, fluid rheology and (positive or negative) tripping speed in the presence of mud circulation at any pump rate. In order to produce meaningful results, the simulator must be able to model general eccentricities, arbitrary Herschel-Bulkley parameters, plus non-zero drillpipe speeds for any pump rate, as the steadystate flow simulator described here will in an exact manner. There are several scenarios that must be considered in addressing this problem which are outlined in Fig. 4-6b. Surge situations, as shown in diagrams (a) and (b), are straightforward to model. In (a) without mud flow, the net flow Q > 0 simply flows to the right. When mud is pumped down the drillstring, as shown in (b), the flow rate Q is simply increased, as shown by the exaggerated velocity profile. Swab scenarios are slightly more subtle. In (c) without mud flow, pulling the drillstring out of the hole induces a negative flow Q < 0 to the left. In (d), mud is pumped down the drillstring at a low pump rate. If the rate is low enough, O will still be negative. On the other hand, if the pump rate is high, as suggested in (e), the net flow will come out of the hole, with Q > 0 now being positive. In this limit, pulling the drillstring out of the hole is consistent with pressures at the bit that exceed those at the surface. These five scenarios are obvious in retrospect, and we have summarized them only because they do not arise in more conventional studies where mud does not circulate. Note that the equation " $P_{bit} = - L \ \partial P / \partial z + P_{surf}$ " is all that is necessary to calculate pressure at the bit. Again, L is the hole or drillstring length, P_{surf} is the known pressure at the

surface choke, and $\partial P/\partial z$ represents output produced by the simulator.

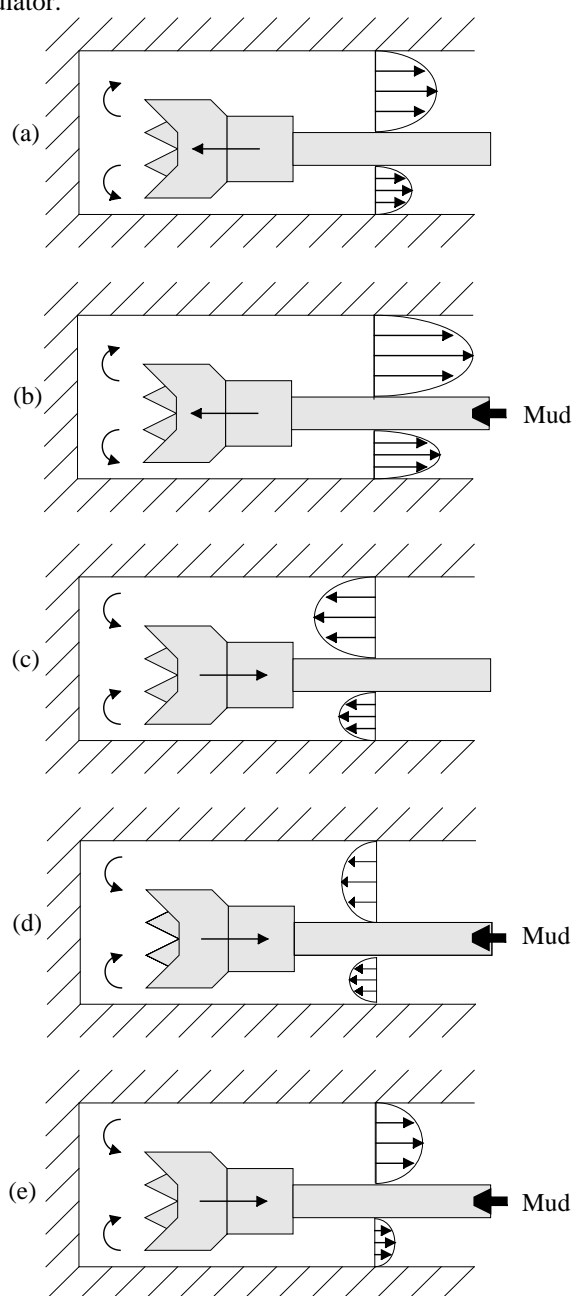


Fig. 4-6b – Five scenarios in continuous flow managed pressure drilling.

Macroscopic rheological properties. Unlike Newtonian flows where the viscosity is a constant once and for all (assuming no pressure or temperature dependencies), the apparent viscosity in a non-Newtonian flow varies throughout the cross-section, and depends on geometrical details plus flow rate or pressure gradient. This is not to say that it is unimportant: it is a useful correlator for cuttings transport and hole cleaning efficiency and may be significant in stuck pipe assessment. Apparent viscosity, we emphasize, is not a property intrinsic to the fluid, however, for Herschel-

Bulkley fluids, "n," "K" and " τ_0 " are. These "microscopic" properties are inputted into the simulator to created an all-important "pressure gradient vs flow rate curve" that describes "macroscopic" properties for the overall flow. This curve is important to swab and surge analysis: once the combined flow rate due to surface pumping plus tripping is known, it gives the pressure gradient required for use in the equation " $P_{bit} = -L \ \partial P/\partial z + P_{surf}$." We will give examples of different curves obtained for different fluid types and annular geometries next. We will introduce the basic analysis concepts by way of software modules that have been developed to host the calculations.

Newtonian fluids. The three Herschel-Bulkley parameters noted above can be determined from viscometer measurements using any number of regression techniques available in the literature (for zero-yield flows of Newtonian and power law fluids, n and K can be determined using integrated software utilities). Once these are available, they are entered into the top right text boxes of the simulator interface in Fig. 4-6c-1 where, for the present example, we have assumed the properties of water at 1 cp. concentric geometry indicated, clicking on "QuikSim" leads to a flow rate of 943.5 gpm. Next, in Fig. 4-6c-2, we increase the eccentricity ε from 0.0 to 0.667 for the same input parameters, and obtain the greatly increased flow rate of 1,521 gpm (it is well known that increases in eccentricity generally lead to increases in flow rate under the same assumed pressure gradient). Figures 4-6c-1 and 4-6c-2 represent the results of "single analysis mode" simulations when detailed results like those in Fig. 5b are required. Much quicker results are obtained when the option in Fig. 4-6c-3 is selected. This option ignores the "pressure gradient specified" or "flow rate specified" prescriptions, and leads, within a minute or two, to the results in Fig. 4-6c-4, here for the eccentric annulus. It is important to observe two features characteristic of Newtonian flows. First, the "pressure gradient vs flow rate curve" passes through the origin; second, the curve is a straight line whose slope depends only on the geometry of the annulus. Once this slope is determined for a specific eccentric annulus at any given pressure gradient, either computationally experimentally, the same applies to all pressure gradients. In this sense, Newtonian flows represent an exception to general nonlinear fluid rheologies, where every case must be treated on an individual basis. The straight line nature of the curve means that changes in flow rate lead to proportional changes in pressure gradient.

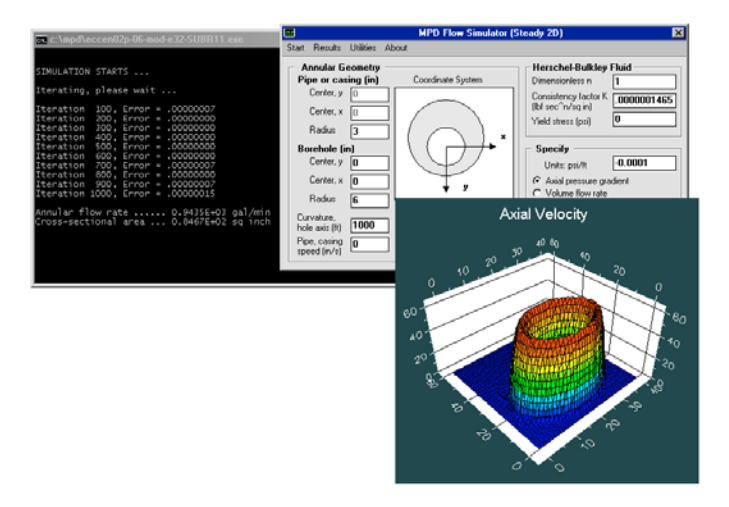


Fig. 4-6c-1 – Newtonian concentric ($\varepsilon = 0.0$) flow.

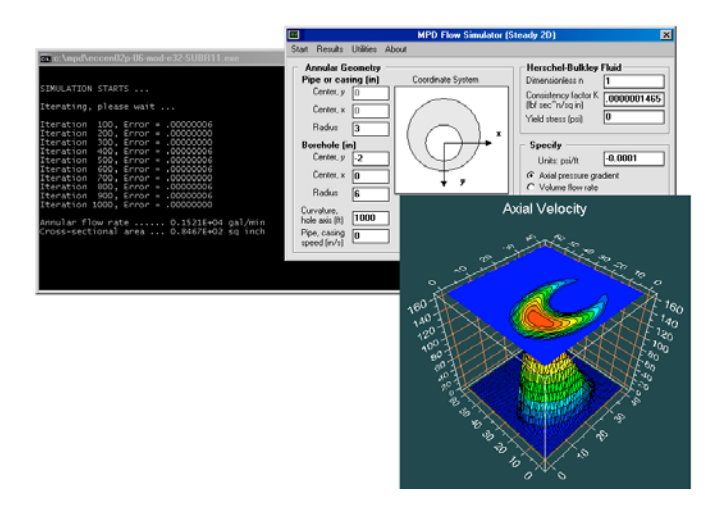


Fig. 4-6c-2 – Newtonian eccentric (ϵ = 0.667) flow.

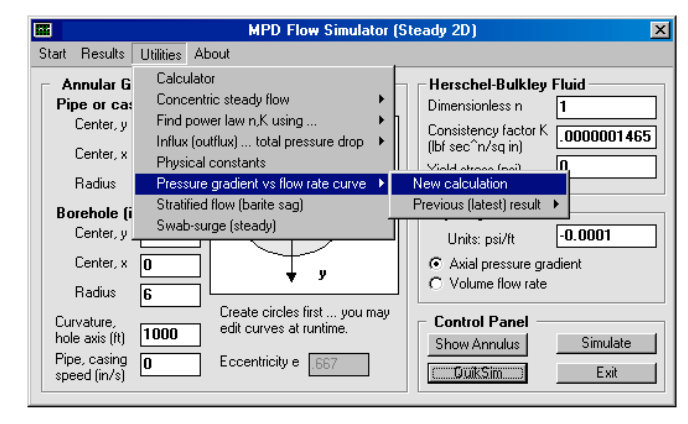


Fig. 4-6c-3 – Newtonian dp/dz vs flow rate calculation (ε = 0.667).

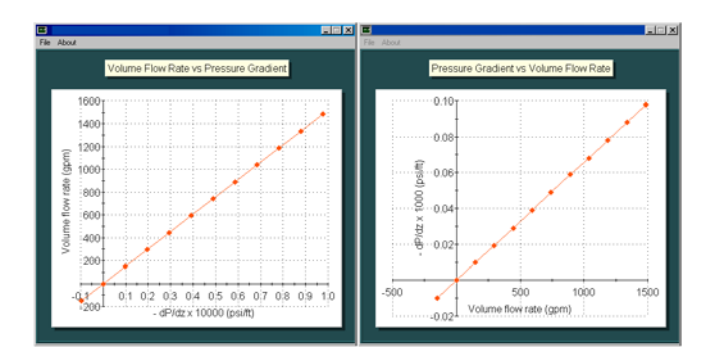


Fig. 4-6c-4 – Newtonian dp/dz vs flow rate behavior (ε = 0.667).

Finally, we note that for the "pressure gradient vs flow rate curve" option in Fig. 4-6c-3, we had fixed the pipe or casing speed to zero for the calculations. In general, this can be a positive or negative constant, making the resulting curve useful in swab-surge applications when tripping at rapid speeds (compared to a nominal speed in the annulus). We will give example calculations later in this example.

Power law fluids. Next we reconsider the above concentric and eccentric geometries for zero-yield power fluids with n=0.415 and K=0.0000944 lbf sec^n/in^2 (this unweighted mud was used in a recent laboratory study). The significant departure of 'n' from unity implies large nonlinearities. This is reflected in the highly curved lines found in Figures 4-6d-1 and 4-6d-2, showing that incremental changes in flow rate do not lead to proportional changes to pressure gradient – the exact changes are rate dependent. Also note the significant differences going from concentric (vertical well) to eccentric (deviated or horizontal well) applications. These results serve as a warning that models based on oversimplified geometric assumptions can lead to operational hazards.

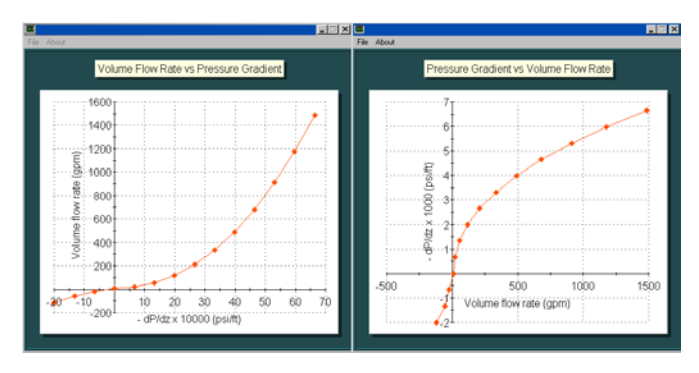


Fig. 4-6d-1 – Power law concentric flow ($\varepsilon = 0.0$).

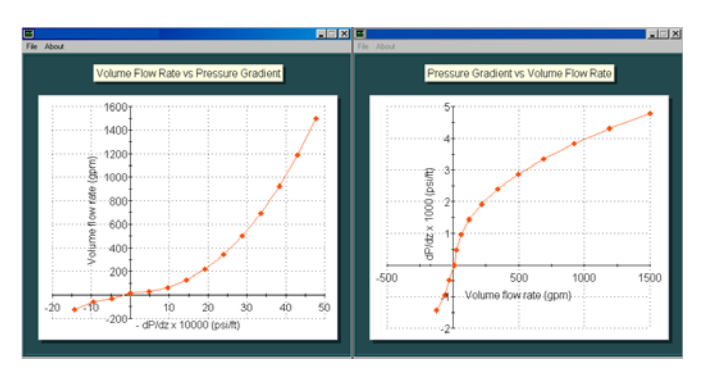


Fig. 4-6d-2 – Power law eccentric flow (ε = 0.667).

Swab and surge examples. Now we consider an application for "tripping with pumps off" and also "with continuous circulation" which demonstrates the subtleties of flow nonlinearity. If we invoke the "Swab-surge (steady)" option from the utilities menu in the main "Steady 2D" interface, we obtain the Swab-Surge Worksheet in Fig. 4-6e-1 (the embedded calculations conservatively assume that the drillbit completely blocks the annulus and that fluid does not pass through the nozzles). We at first turn off the mudpump while assuming a hole radius of 4 in and a "tripping in" speed of 5,000 ft/hr. The Worksheet indicates that, following the convention of Fig. 4-6a, we have a positive induced flow rate of +217.6 gpm while the drillpipe speed is negative with a value of -16.67 in/sec (the drillbit is assumed to completely block the hole). The Worksheet instructs the user to enter "217.6" and "-16.67" as we have in Fig. 4-6e-2 for the eccentric annulus and power law fluid assumed. Clicking on "Show Annulus" produces the display in Fig. 4-6e-3. Then the required axial pressure gradient ∂P/∂z is – 0.006494 psi/ft (minus values indicate high surge pressures at the bit).

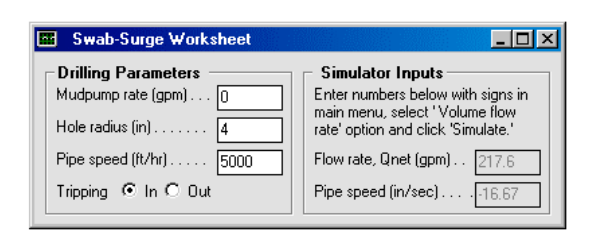


Fig. 4-6e-1 - Assumptions for surge run with pumps off.

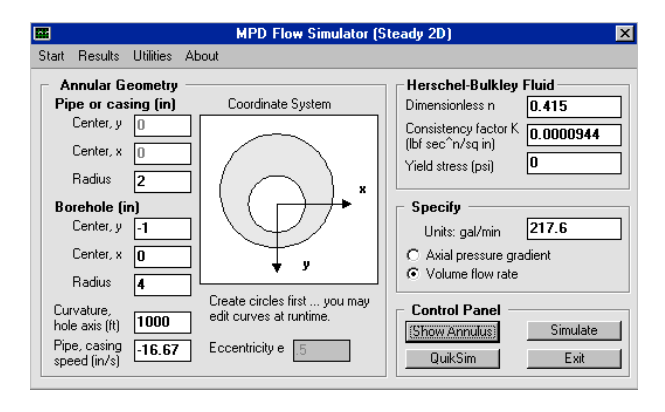


Fig. 4-6e-2 – Additional assumptions, surge run with pumps off.

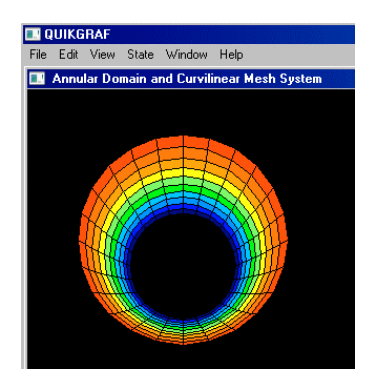


Fig. 4-6e-3 – Eccentric annulus and curvilinear grid assumed (internal grid used in computations is finer).

Swab-Surge Worksheet	_ D X
Drilling Parameters Mudpump rate (gpm)	Simulator Inputs Enter numbers below with signs in main menu, select 'Volume flow rate' option and click 'Simulate.' Flow rate, Qnet (gpm) 717.6 Pipe speed (in/sec)16.67

Fig. 4-6e-4 – Assumptions for surge run with pumps on.

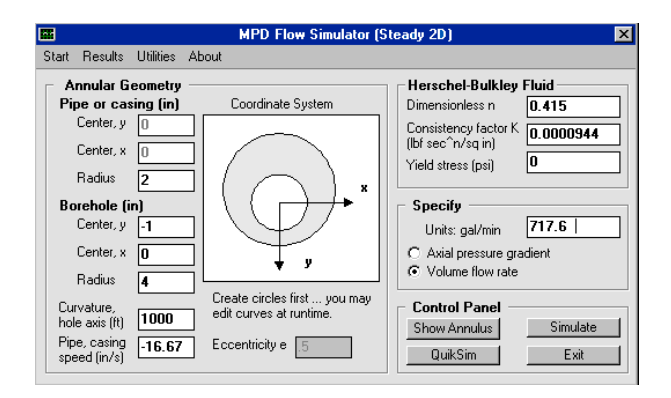


Fig. 4-6e-5 - Additional assumptions, surge run with pumps on.

Now, consider an identical situation except that the pump is circulating at 500 gpm. The screens analogous to Figures 4-6e-1 and 4-6e-2 are given above. Clicking on "QuikSim" (as before) shows that the required pressure gradient now becomes – 0.01045 psi/ft. This pressure drop is steeper than before, as expected, because the flow rate is higher. It is interesting that the flow rate ratio between the two runs above is 717.6/217.6 or 3.30. The ratio of pressure gradients, however, is 0.01045/0.006494 or 1.61. In a Newtonian flow, the "3.30" and "1.61" numbers would have been identical. For non-Newtonian flows, they typically are not, and general conclusions cannot be given – results must be found by case-by-case computations. This example points to the danger of using Newtonian models even for crude estimates.

In the next calculation, we consider "tripping out" in a swab application with the mud pumps off. Instead of "+217.6" and "-16.67" as we had before, Fig. 4-6e-6 shows that the relevant numbers are reversed, with "-217.6" and "+16.67." When these replace their counterparts in Fig. 4-6e-

2, "QuikSim" analysis correctly shows that the applied pressure gradient is now + 0.006494 psi/ft instead of the previous – 0.006494 psi/ft. This positive sign, as discussed earlier, indicates lower pressures relative to those at the surface. Now let us recall the equation " $P_{bit} = -L \partial P/\partial z + P_{surf}$ " for pressure at the drillbit. Suppose that $P_{surf} = 14.7$ psi is open to the atmosphere. Then, we can express bit pressure in psi if L is given in feet via $P_{bit} = 14.7 - 0.006494$ L. In this example, P_{bit} vanishes if L = 2,264 feet, at which point the possibility of a blowout increases significantly.

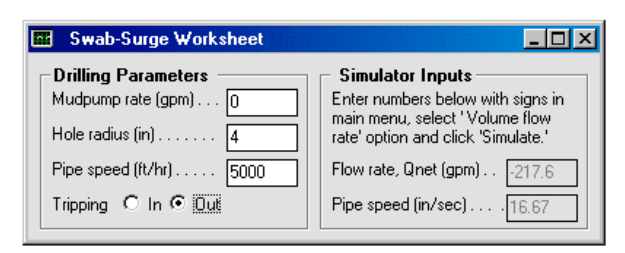


Fig. 4-6e-6 - Assumptions for swab run with pumps off.

What would be the effect if, as in Fig. 4-6e-4, we ran the mudpump at 500 gpm? The corresponding Swab-Surge Worksheet would appear as it does in Fig. 4-6e-7, showing a net flow rate of 282.4 gpm. The calculation suggested by Fig. 4-6e-8 gives a negative pressure gradient of – 0.005811 psi/ft. This shows that the 500 gpm pump rate is enough to prevent overly low pressures when tripping out at 5,000 ft/hr. While we have focused on low pressures that may allow blowouts, it is obvious that a similar analysis allows us to select pump rates that will not fracture the formation when the fracture gradient is known.

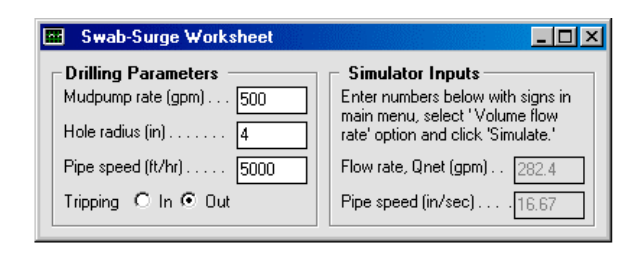


Fig. 4-6e-7 – Assumptions for swab run with pumps on.

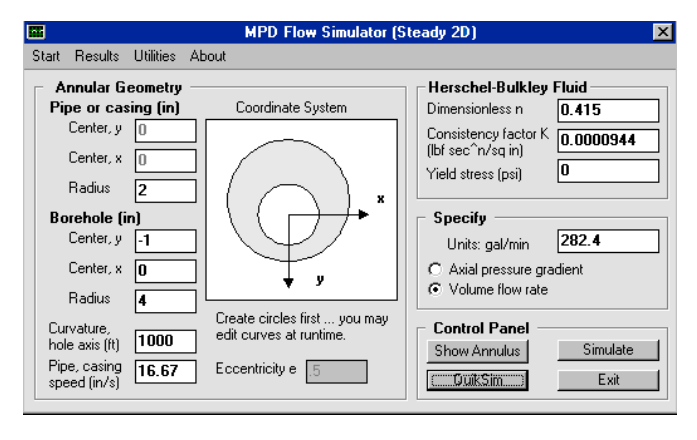


Fig. 4-6e-8 - Additional assumptions for swab run with pumps on.

Neutral pressure gradient operation. The simulator allows us to pose and solve still another problem of interest in swabbing operations. Suppose, as in the above, we wish to trip out at 5,000 ft/hr or 16.67 in/sec. We found from a prior analysis that this action is responsible for a negative flow rate of – 217.6 gpm, with the left-bound annular fluid flow arising from the need to fill the borehole void left by the retreating drillstring. We ask which net flow rate would allow us to maintain a "neutral pressure gradient" of 0.00 psi/ft, that is, one that allows us to have a constant pressure along the annulus equal to the surface choke pressure. If we run the simulator with +16.67 in/sec and 0.00 psi/ft in "specify axial pressure gradient" mode, we obtain a net flow rate of 53.52 gpm. This 53.52 gpm is, of course, the flow rate obtained by simply dragging the drillstring along without an imposed pressure gradient. In other words, the pump must be operated at 217.6 + 53.52 or 271.1 gpm to create a simple dragging flow and to produce the required zero pressure gradient.

This "reverse thinking" can be verified directly. It is easily validated by the forward calculation in Fig. 4-6e-9. This calls for us to enter 53.52 in the volume flow rate screen of Fig. 4-6e-10. Clicking "QuikSim" leads to an extremely small value of – 0.00001221 psi/ft which allows us to impress surface choke pressure directly on the drillbit. Pressure is constant along the borehole. This predictive capability is a direct result of the ability to model drillpipe movement in a rigorous computational manner in very complicated borehole environments. We again note that the simulator was applied to a highly nonlinear power law fluid with pipe movement in a very eccentric annulus.

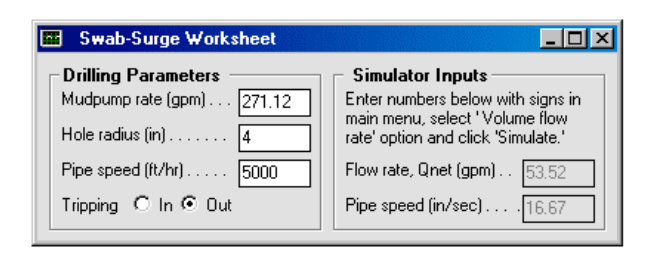


Fig. 4-6e-9 – Surface mudpump rate needed for vanishing axial pressure gradient while tripping out.

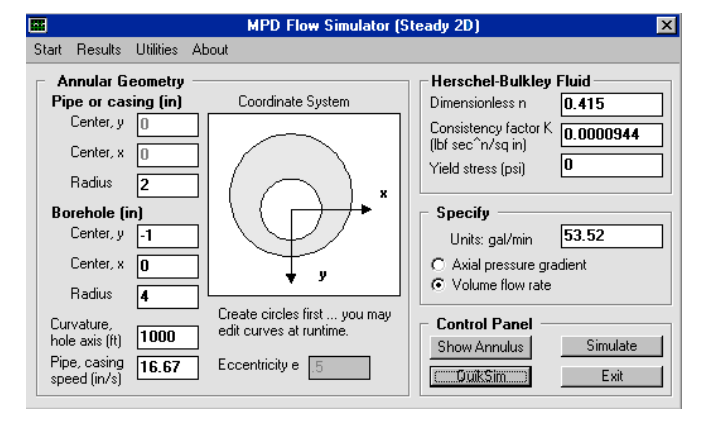


Fig. 4-6e-10 - Calculation providing zero axial pressure gradient.

Example 4-7. Steady-state swab-surge in concentric annuli for power law fluids with drillpipe rotation and slow pipe movement.

The approach taken to model swab-surge effects in Example 4-6 is straightforward. Basically, the Swab-Surge Worksheet is used to compute a kinematic volume flow rate correction to the mud pump flowrate that accounts for changes in void space near the drillbit due to tripping out or in. The new flow rate is then used in the annular flow analysis together with the correctly signed drillpipe speed. We employ this approach throughout for swab-surge applications. When the drillpipe rotates, a closed form analytical solution for the complete flowfield can be developed which allows general steady rotation at any rpm provided the annulus is concentric and stationary in the axial direction. This latter assumption is satisfactory for slow tripping speeds, as they invariably should be in operations, given safety considerations. The simpler simulator is accessed as shown in Fig. 4-7a.

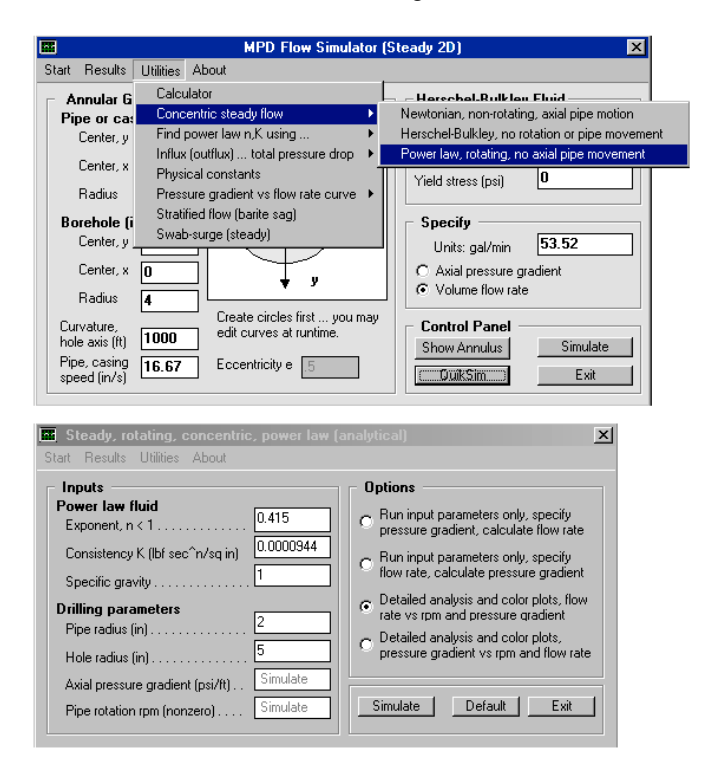


Fig. 4-7a – Concentric, rotating, power law flow.

Four run-time options are shown in the above screen. The first two provide detailed results for single run-sets. The third and fourth options provide fast calculations for "GPM vs RPM and dP/dz" and "dP/dz vs RPM and GPM," typically requiring about fifteen seconds of computing time, with automated three-dimensional color plots that allow zooming and mouse rotation. Results shown in Figures 4-7b,c clearly illustrate the roles of rotation and pressure gradient that must be understood in managed pressure drilling applications.

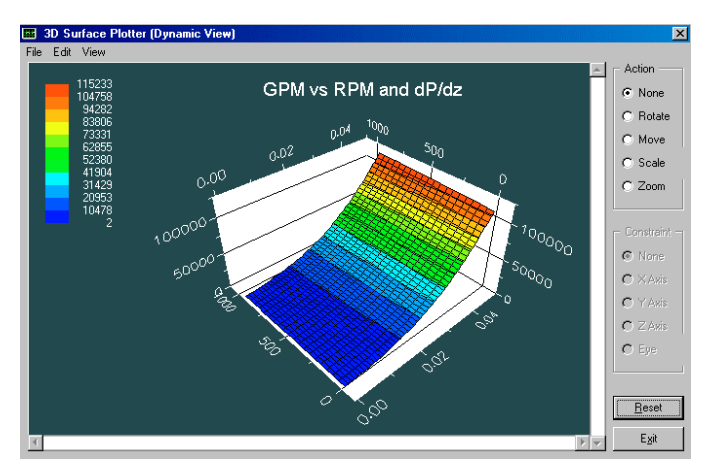


Fig. 4-7b - GPM vs RPM and dP/dz.

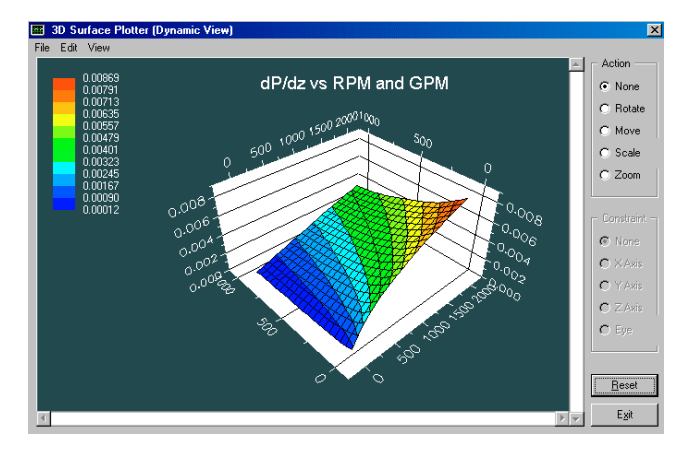


Fig. 4-7c – dP/dz vs RPM and GPM.

We emphasize that the foregoing results are for concentric annuli. For such problems, certain inertial terms in the axial momentum flow equation vanish identically and non-Newtonian effects enter only through shear-thinning. When eccentricity is important, the fully transient solvers can be used to model not only unsteady flows, but steady flowfields induced by constant rotation rates. Figures 4-7d and 4-7e display typical computed results for a highly eccentric annulus. In these calculations, a spatially-dependent inertial correction to pressure gradient (which is proportional to fluid density and rotation rate, and inversely proportional to apparent viscosity) acts in such a way that the point of maximum axial speed (normally at the widest part of the annulus) now shifts azimuthally.

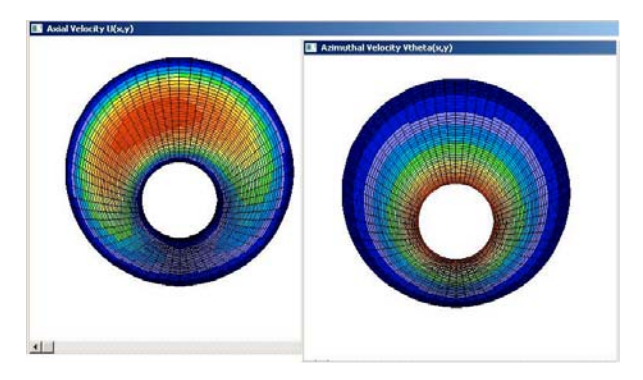


Fig. 4-7d – Maximum axial velocity location shifts sideways as pipe rotates (left), azimuthal velocity field (right).

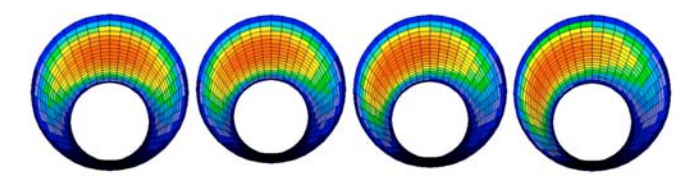


Fig. 4-7e – Axial velocity distribution as rotation rate increases from left to right from 0 to 400 rpm.

Example 4-8. Steady-state swab-surge in eccentric annuli for Herschel-Bulkley fluids with drillpipe rotation and axial movement.

In Example 4-7, we addressed pressure gradient computations for general flow rates and rotation speeds for power law fluids in a concentric annulus under steady conditions without axial pipe movement. For such flows, the convective terms in the momentum equations vanish identically. The effect of rotation is restricted to shearthinning so that, for a given pressure gradient, increases in rotation rate will reduce apparent viscosity and increase volumetric flow. These effects are well known in the older literature and apply mainly to vertical wells.

Run A. In deviated and horizontal wells, annular eccentricity is the rule, and while shear-thinning remains important, a nonlinear convective term (whose magnitude is proportional to fluid density and pipe rotation speed and inversely proportional to apparent viscosity, and which is variable throughout the annular cross-section) appears and modifies the local axial pressure gradient. For most practical geometries, this will reduce the flow relative to that found for the eccentric non-rotating problem for the same applied pressure gradient. Equivalently, for the same flow rate, the pressure drop increases significantly. These properties are important in managed pressure drilling.

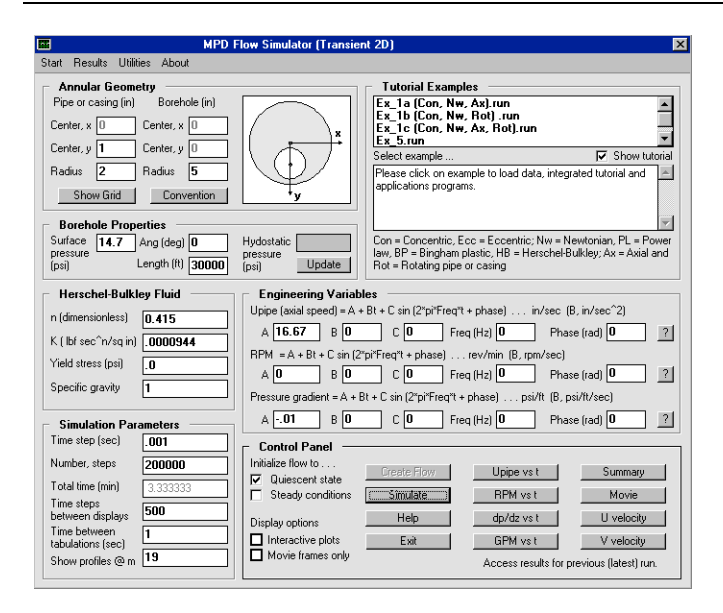


Fig. 4-8a-1 - Transient 2D flow menu (no rotation).

The direct computation of steady rotating flow in an eccentric annulus is often an unstable numerical process if calculated from a purely steady formulation. Solutions have been published by various authors who have all given few computational details related to convergence properties and computing times. Such schemes tend to destabilize at higher specific gravities and rotation speeds, and unfortunately, in the ranges typical of most drilling applications. Fortunately, steady rotating flow solutions can be stably computed by solving the transient formulation asymptotically for large times. In Fig. 4-8a-1, we have set up flow simulations for a power law fluid in an eccentric annulus with axial pipe movement but no rotation. The problem is integrated in time starting with quiescent conditions. Fig. 4-8a-2 shows computed volume flow rates reaching constant levels at 941.0 gpm after about one minute of computing time (this is interestingly, but fortuitously, also the physical time scale) with convergence to steady-state achieved very stably. The maximum axial flow speed is found, as expected, at the wide side of the annulus.

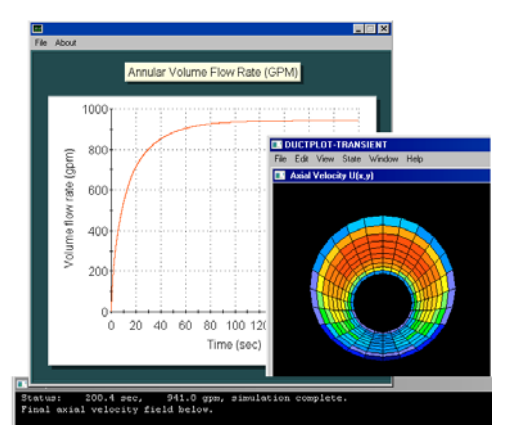


Fig. 4-8a-2 - Eccentric power law results without pipe rotation.

Run B. Repeating the foregoing simulation to allow drillstring rotation is straightforward. For example, we simply change the "0" in the RPM box to "100" (as seen from Fig. 4-8b-1) and completely automated calculations lead to a reduced flow rate of 562.2 gpm as shown in Fig. 4-8b-2. As is well known, the location of maximum axial velocity moves azimuthally, and the results are consistent with this observation, a fact that may be useful in cuttings transport and hole cleaning applications. Computed results also indicate that the time to reach equilibrium decreases with rotation. The results presented here, for pipe moving both axially and azimuthally, show that pressure gradient calculations are doable and straightforwardly performed for general power law fluids in highly eccentric annuli.

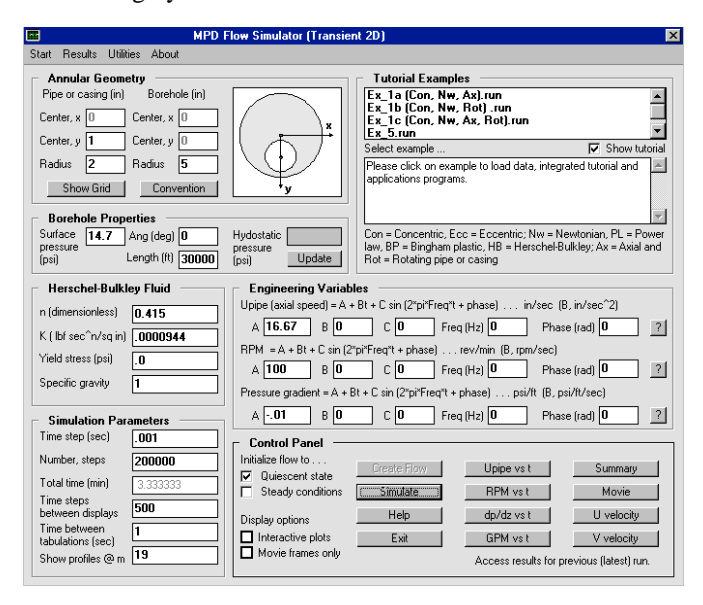


Fig. 4-8b-1 – Modified flow with 100 rpm drillstring rotation.

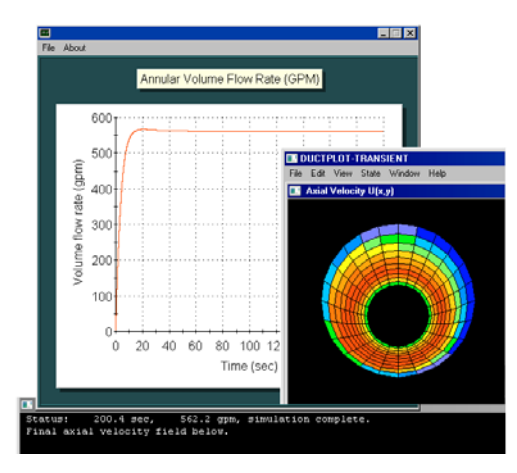


Fig. 4-8b-2 - Reduced flow rate achieved in shorter time.

Run C. In the next calculation, we repeat that in Fig. 4-8b-1, which included axial pipe movement and nonzero rotation speed in addition to borehole eccentricity and non-Newtonian power law flow, but now consider the additive effects of Herschel-Bulkley yield stress. In Fig. 4-8c-1, we

modify the previous "0" to "0.002 psi" and leave all other parameters unchanged. As before, the calculations require about 30 seconds and are performed stably.

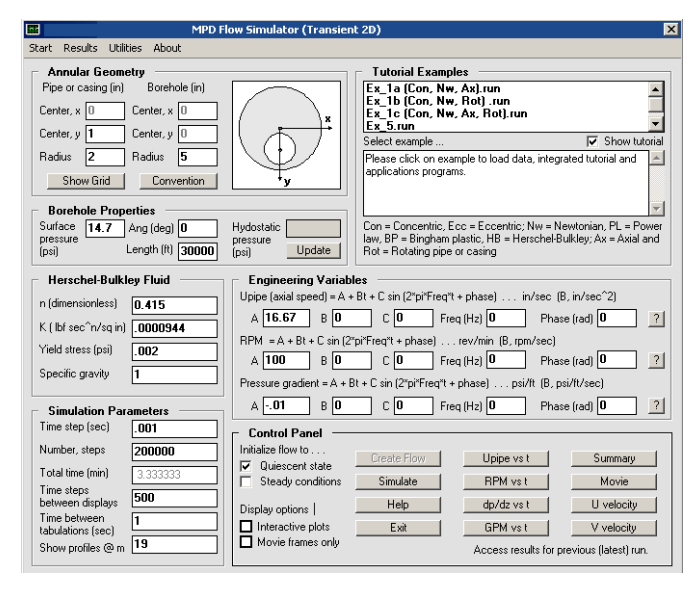


Fig. 4-8c-1 - Flow at 100 rpm now with 0.002 psi yield stress.

Fig. 4-8c-2 shows that the volume flow rate is reduced from 562.2 gpm to 516.9 gpm, for a 9% reduction. One might have asked what the required pressure gradient would be for the yield stress fluid if we needed to maintain a 562 gpm flow rate. For the steady flow solver, direct "pressure gradient specified" and inverse "flow rate specified" calculation modes were available. For mathematical reasons, this is not practical for transient simulations. A simple procedure requires us to manually attempt reasonable pressure gradient guesses. This procedure can be very efficient. For this example, the author determined that – 0.011 psi/ft would yield 562 gpm after three tries or about two minutes of desk time. In other words, the presence of yield stress steepened the pressure gradient by a substantial 10%.

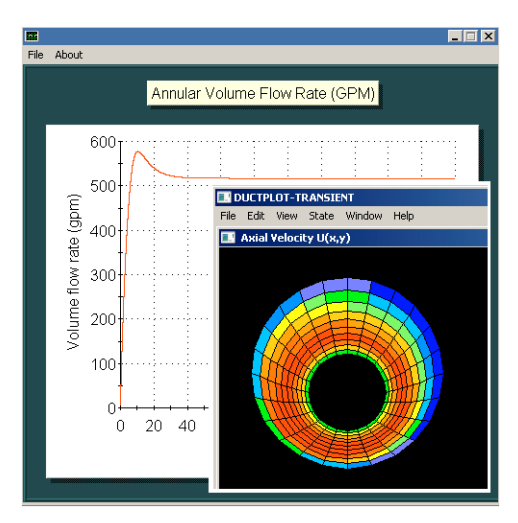


Fig. 4-8c-2 - Flow at 100 rpm now with 0.002 psi yield stress.

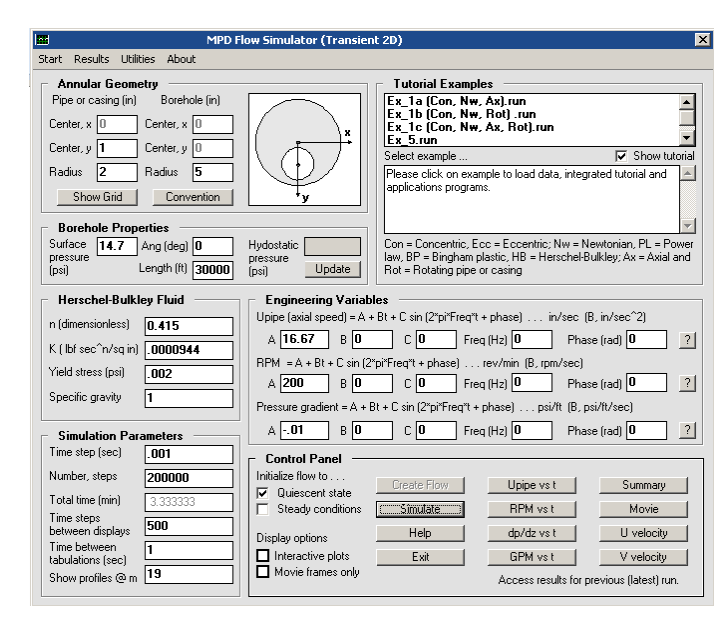


Fig. 4-8d-1 - Flow at 200 rpm with 0.002 psi yield stress.

Run D. Next, we will re-consider the yield stress problem in Fig. 4-8c-1 and determine the consequences of increasing rotation rate from 100 to 200 rpm. The input screen is shown in Fig. 4-8d-1. The effect of doubling rotation speed is a decreased flow rate for the same – 0.01 psi/ft, in this case a much smaller 443.3 gpm, as shown in Fig. 4-8d-2. This effect arises from eccentricity. And what if we had insisted on 562 gpm? Then, some simple manual "cut and try" calculations with different pressure gradient guesses lead to a substantially steepened – 0.0131 psi/ft, a value that was obtained within two minutes with four different guesses.

Favorable effect of rotation on hole cleaning. The detailed effects of rotation and yield stress have been discussed in the context of eccentric borehole annuli with coupled axial drillstring movement. These calculations represent completely new industry capabilities. interesting to note that, from Fig. 4-8a-2 for non-rotating flow, the location of maximum axial flow speed lies symmetrically at the top at the wide side of the eccentric annulus. When rotation exists, as shown in Figures 4-8b-2, 4-8c-2 and 4-8d-2, the location of the maximum moves azimuthally as shown, consistently with other known investigations (note that "red" in these three diagrams denote different speeds). increased relative speeds are achieved at the bottom of the annulus is consistent with the improved hole cleaning ability of drillstrings under rotation observed under many field conditions. Of course, this improvement comes at the expense of steepened pressure gradients, a crucial trade-off whose value must be assessed by the drilling engineer. The end decision made at the rigsite will depend on "the numbers" which can only be obtained computationally.

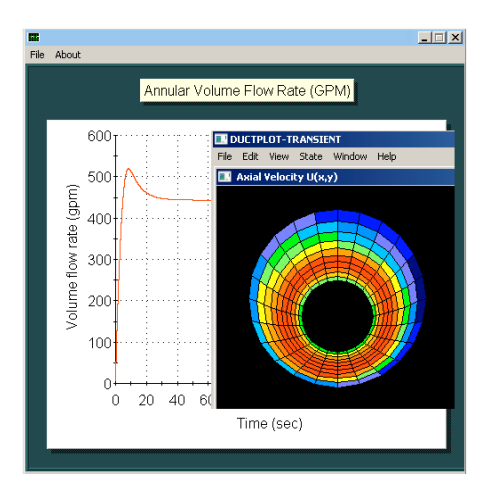


Fig. 4-8d-2 - Flow at 200 rpm with 0.002 psi yield stress.

Here we study the effect of slow-down in drillstring rotation rate (the menus support more complicated motions, e.g., stick-slip torsional oscillations). Acceleration and deceleration are always encountered in start-up and slowdown. We repeat the calculation of Fig. 4-8d-1, starting with 200 rpm for the nonzero yield stress fluid. But as shown in Fig. 4-8e-1, we allow the 200 rpm to slow down to 0, as seen from the "- 0.5" deceleration rate selected under the RPM menu. Clicking on "?" to the right produces a plot of the assumed RPM vs time curve in Fig. 4-8e-2 (note that numerous time functions for axial pipe speed, rotation rate and pressure gradient are permissible with the simulator). The calculated flow rate vs time response is shown in Fig. 4-8e-3. This flow rate increases as expected, with drillstring rotation rate decreasing. In this transient simulation, the location of maximum axial velocity is not stationary, but instead propagates azimuthally about the eccentric annulus. "snapshot" at one instant in time is shown in Fig. 4-8e-4. Although this example is purely transient, we have included it in the steady eccentric annular flow example to highlight the importance (or perhaps, unpredictability) of transient effects. The shape of the transient rate curve in Fig. 4-8e-3, we emphasize, is obtained for a simple Herschel-Bulkley fluid and not one with "memory" effects.

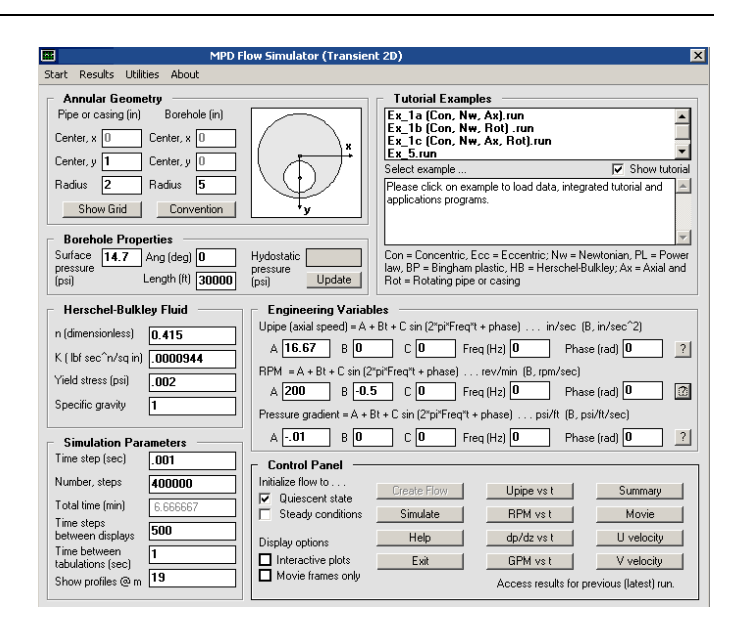


Fig. 4-8e-1 – Decreasing rotation rate, from 200 to 0 rpm.

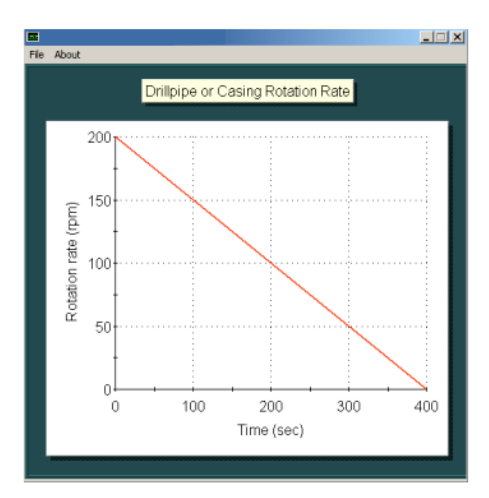


Fig. 4-8e-2 - Linearly decreasing rpm, from 200 to 0.

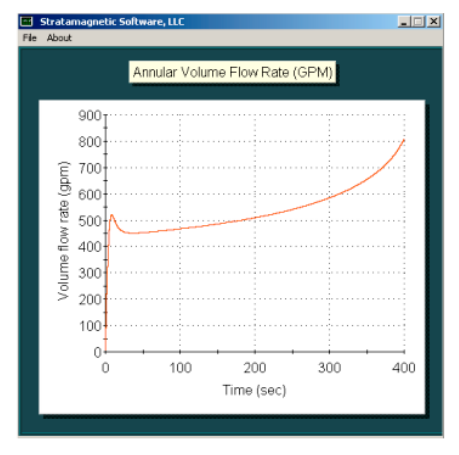


Fig. 4-8e-3 – Transient increasing flow rate with decreasing rpm.

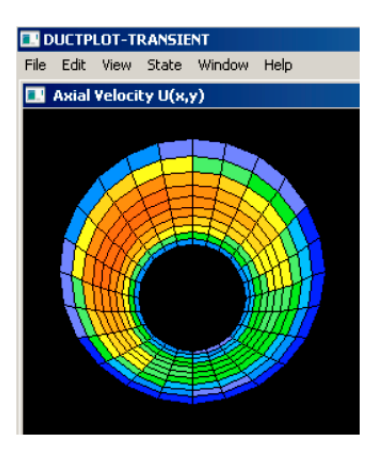


Fig. 4-8e-4 – Transient movement of maximum point as rpm decreases.

Run F. In this final example, we consider a complete steady swab-surge application with high annular eccentricity, a nonlinear yield stress fluid, and allow the drillpipe to move axially while simultaneously rotating. This demonstrates the capabilities in the math models and provides a complete summary of the software menu sequences needed to perform similar calculations. In order to proceed, the "Swab-Surge Worksheet" must be invoked from the main "MPD Flow Simulator (Steady 2D)" in Fig. 4-8f-1. In the Worksheet, we consider a five-inch radius hole and a pipe trip-out speed of During this operation, we wish to pump continuously, with the surface mudpump rate set at 856.9 gpm. Now, as the drillpipe is withdrawn from the hole, fluid must rush in to fill the bottomhole void. The Worksheet indicates that the effective annular flow rate is 516.9 gpm and that the pipe speed in "inch/sec" units is 16.67 in/sec.

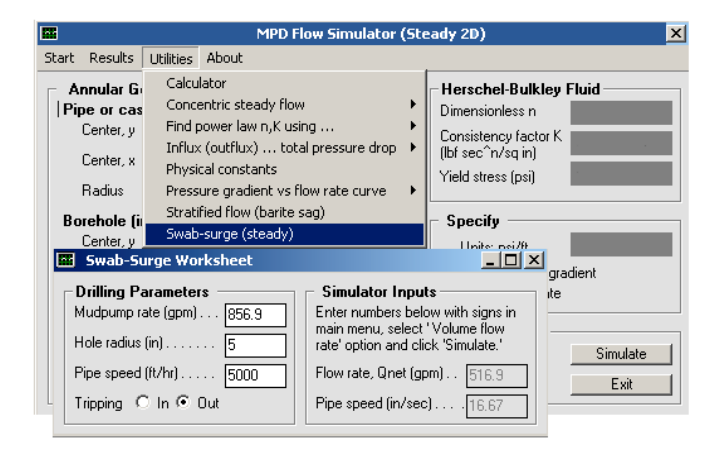


Fig. 4-8f-1 – Running the "Swab-Surge Worksheet" (areas that do not affect Worksheet calculator are shown shaded).

Now, we wish to focus this study the non-Newtonian flow of a Herschel-Bulkley fluid with n = 0.415, K = 0.0000944 lbf sec^n/in^2 and $\tau_0 = 0.002$ psi, in an annulus formed by a 4 in diameter pipe in a 10 inch diameter hole, with an eccentricity of 0.3333. We will demonstrate the solution process for flows without and with rotation. If we

wish to consider axial movement only but without rotation, we can run the steady flow calculation shown in Fig. 4-8f-2 in "volume flow rate specified" mode. Clicking on "QuikSim" produces the screen output iteration history shown on the following page.

```
SIMULATION STARTS ..
      Herschel-Bulkley model, with exponent "n" equal
      to 0.4150E+00 and consistency factor of 0.9440E-04
      lbf sec^n/sq in.
      A yield stress of 0.2000E-02 psi is taken.
      Borehole axis radius of curvature is 0.1000E+04 ft.
      Axial speed of inner pipe is 0.1667E+02 in/sec.
      Target flow rate of 0.5169E+03 gal/min specified.
      Iterating on pressure gradient to match flow rate ...
      Iteration
                 100, Error = .00672962
      Iteration
                 200, Error = .00248959
                 300, Error =
      Iteration
                               .00119476
      Iteration
                 400, Error =
                               .00052236
      Iteration
                 500, Error =
                               .00019270
      Iteration
                 600. Error =
                               .00005923
      Iteration
                 700, Error =
      Iteration
                 800, Error = .00000521
                 900, Error = .00000171
      Iteration
      Iteration 1000, Error = .00000047
        Axial pressure gradient of -.1000E+00 psi/ft
         vields volume flow rate of 0.4076E+06 gal/min.
      Flow rate target error is 0.7876E+05 %
                 100, Error = .00371665
      Iteration
      Iteration
                 200, Error = .00067117
      Iteration
                 300, Error =
      Iteration
                 400, Error =
      Iteration
                 500, Error =
                 600. Error =
      Iteration
                               .00000192
      Iteration
                 700, Error =
      Iteration
                 800, Error = .00000010
                 900, Error = .0000010
      Iteration
      Iteration 1000, Error = .00000010
         Axial pressure gradient of -.5000E-01 psi/ft
         vields volume flow rate of 0.4141E+05 gal/min.
      Flow rate target error is 0.7911E+04 %
         Axial pressure gradient of -.6250E-02 psi/ft
         yields volume flow rate of 0.6708E+03 gal/min.
      Flow rate target error is 0.2977E+02 %
      Iteration 100, Error = .00000000
                 200, Error = .00000011
      Iteration
      Iteration
                 300, Error = .00000000
      Iteration
                 400. Error =
                               .00000011
      Iteration
                 500, Error = .00000011
                               .00000011
      Iteration
                 600, Error =
      Iteration
                 700, Error = .00000000
      Iteration
                 800, Error = .00000021
      Iteration
                 900, Error = .00000011
      Iteration 1000, Error = .00000000
      O Axial pressure gradient of -.4688E-02 psi/ft
         yields volume flow rate of 0.5217E+03 gal/min.
                 gradient.
      Pressure
                           found
                                  iteratively.
                                                   - 4688E-02
psi/ft,
      to yield 0.5217E+03 gal/min vs target 0.5169E+03
gal/min.
```

Note: Iterations terminate within 1% of target rate.

Refine result by manually changing pressure gradient.

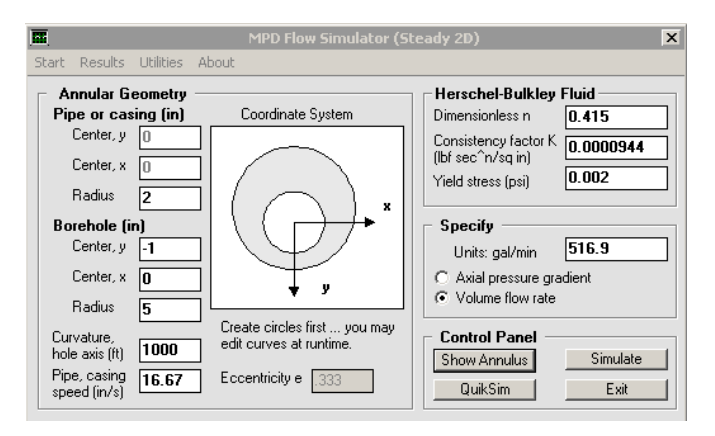
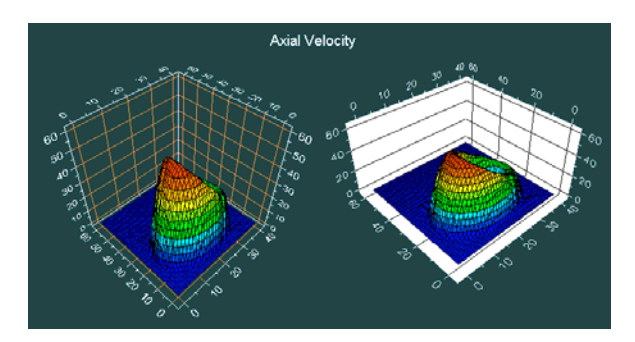


Fig. 4-8f-2 - Steady 2D solver.



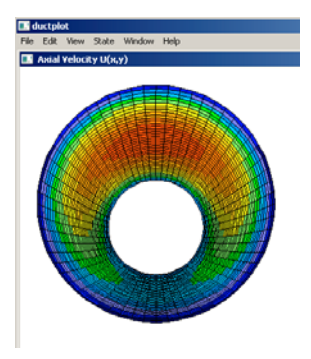


Fig. 4-8f-3 – Computed axial velocity (non-rotating).

In other words, the pressure gradient associated with the non-rotating flow is - .004688 psi/ft. The corresponding axial velocity field is shown in Fig. 4-8f-3 in a variety of available plots. Note that for non-rotating flows, the "Steady 2D" solver automatically computes the required pressure gradient using an internal inverse procedure. It has not been possible to develop a steady solver that allows rotation which is also unconditionally numerically stable. This does not, fortunately, mean that steady rotating flows cannot be computed.

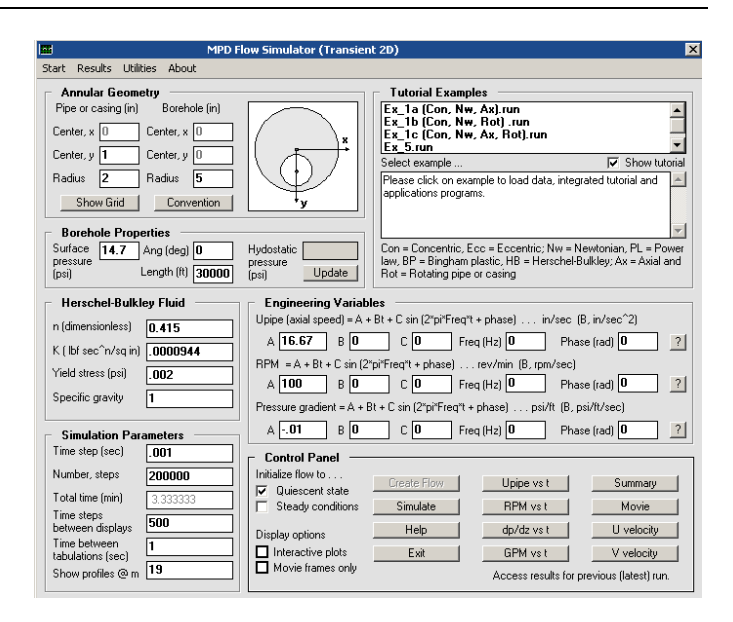


Fig. 4-8f-4 - Transient 2D solver.

We demonstrate how by considering the effect of a moderate 100 rpm rotation rate. We use the "Transient 2D" solver in Fig. 4-8f-4, with input boxes completed for the same simulation parameters. The strategy is to solve a fully transient problem until steady-state behavior is obtained. Because a "flow rate specified" mode is not available for transient calculations, one resorts to repeated guesses for pressure gradient, but we have found that three or four will usually lead to a flow rate within 1-2% of the target value. Since each trial calculation equilibrates quite rapidly, as shown in Fig. 4-8f-5, the total "desk time" required is often two minutes or less.

For this rotating flow run, a pressure gradient of -0.01 psi/ft is required, as compared to the -.004688 psi/ft obtained in the non-rotating case. In other words, pressure gradients are twice as severe because of rotation. The "Results" menu in Fig. 4-8f-4 provides numerous post-processed results in addition to those of Fig. 4-8f-5. For example, axial and azimuthal velocity distributions are available, as given in Fig. 4-8f-6, as are detailed color plots of different physical properties like apparent viscosity, shear rate and viscous stress.

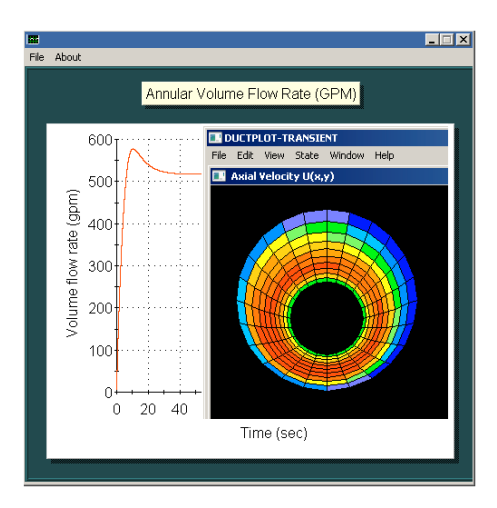


Fig. 4-8f-5 – Flow rate history and velocity distribution (note, maximum axial velocities appear at annular bottom).

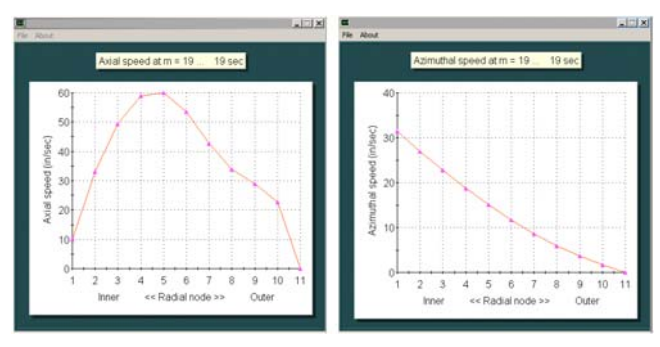


Fig. 4-8f-6 – Axial and azimuthal velocities at cross-section "m = 19."

Closing Remarks

The present paper describes new capabilities in modeling steady and transient non-Newtonian flow in highly eccentric annuli, with or without plug zones associated with yield stress fluids, with realistic geometric anomalies, plus effects like borehole axis curvature and drillpipe translation and rotation. In addition, the option to specify either axial pressure gradient or total volume flow rate is provided. The rigorous fluid-dynamical model formulated here and its exact mathematical solution, augmented by rapidly converging algorithms and convenient color displays, are intended to provide state-of-theart capabilities useful to managed pressure drilling, hole cleaning and cementing: the focus has been swab-surge applications.

Acknowledgments

The authors gratefully acknowledge 2009-2011 support from the United States Department of Energy for their technical proposal "Advanced Steady-State and Transient, Three-Dimensional, Single and Multiphase, Non-Newtonian Simulation System for Managed Pressure Drilling." This effort was administered by the Research Partnership to Secure Energy for America (RPSEA) through its Ultra-Deepwater Program under Subcontract No. 08121-2502-01. The curvilinear grid generation research was also supported by the United States Department of Energy, in particular, under

Small Business Innovation Research Grant DE-FG03-99ER82895 in 1999-2000. We are indebted to Art Schroeder, Energy Valley, to Jim Chitwood, Chevron, and to James Pappas, RPSEA, for their encouragement and advice, and especially to John Lofton, Chevron, for his engineering insights and guidance related to several areas in the modeling of rotating pipe flow effects. The views expressed in this paper represent those of the authors only and not necessarily the opinions of any program sponsors.

References

- Chin, W.C., <u>Borehole Flow Modeling in Horizontal</u>, <u>Deviated and Vertical Wells</u>, Gulf Publishing, Houston, 1992.
- 2. Chin, W.C., <u>Computational Rheology for Pipeline and Annular Flow</u>, Elsevier, Cambridge, 2001.
- 3. Chin, W.C., <u>Quantitative Methods in Reservoir Engineering</u>, Elsevier, Cambridge, 2002.
- Chin, W.C. and Zhuang, X., "Exact Non-Newtonian Flow Analysis of Yield Stress Fluids in Highly Eccentric Borehole Annuli with Pipe or Casing Translation and Rotation," SPE 131234-PP, presented at the CPS/SPE International Oil & Gas Conference and Exhibition, Beijing, China, 8-10 June 2010.
- Souza Mendes, P.R. and Dutra, E.S.S., "A Viscosity Function for Viscoplastic Liquids," Annual Transactions of the Nordic Rheology Society, Vol. 12, 2004.